ACI STRUCTURAL JOURNAL TECHNICAL PAPER

Title no. 103-S83

Behavior and Design of Adhesive Bonded Anchors

by Rolf Eligehausen, Ronald A. Cook, and Jörg Appl

This paper presents the results of extensive numerical and experimental work performed to establish a behavioral model that provides the basis for developing design provisions for anchorages to concrete using adhesive bonded anchors. These types of anchorage systems are used extensively, yet they are currently excluded from the design provisions of ACI 318. The behavioral model is compared with a worldwide database containing 415 tests on adhesive anchor groups, 133 tests of adhesive anchors located near a free edge, and accompanying baseline single anchor tests used to establish the relationship between the results of the group and edge tests and the behavior of isolated single anchors.

Keywords: anchorage; anchors; embedment; fastener.

INTRODUCTION

Anchorages to concrete include cast-in-place and post-installed anchors. Post-installed anchors are either mechanical or bonded anchors. Figure 1 shows the typical types of anchors. The design of anchorages using cast-in-place and post-installed mechanical anchors is discussed in ACI 318-05, Appendix D.[1] Bonded anchors are used extensively in practice but have not yet been incorporated into the design provisions of ACI 318, Appendix D.

The purpose of this paper is to introduce a behavioral model to predict the failure load of anchorage systems with adhesive bonded anchors loaded in tension. It is based on extensive numerical and experimental work that provides a foundation for incorporating design provisions for these types of anchorage systems into ACI 318, Appendix D. The behavioral model is compared to the results of experimental investigations contained in a worldwide database, summarized in Table 1.

DESCRIPTION OF BONDED ANCHORS

Bonded anchors include both adhesive anchors and grouted anchors (Fig. 1). An adhesive anchor is a steel element (threaded rod or deformed bar) inserted into a drilled hole in hardened concrete with a structural adhesive acting as a bonding agent between the concrete and the steel. For adhesive anchors, the diameter of the drilled hole is typically not larger than 1.5 times the diameter of the steel element. Adhesive anchors are available in glass or foil capsule systems using organic compounds and in injection systems using organic or inorganic compounds or a mixture of the two in either pre-packaged cartridge systems or bulk injection systems. A grouted anchor may be a threaded rod, deformed bar, headed bolt, or threaded rod with a nut at the embedded end installed in a large drilled hole with a commercially available pre-mixed grout. Typically, the hole size for grouted anchors is approximately twice the diameter of the anchor and the hole is drilled using a core drill. Because of the large hole diameter, grouted anchors are typically limited to vertical installations. Grout products may be inorganic, organic, or a mixture of the two.

The behavior and design recommendations for single grouted anchors are addressed in Zamora et al.[2] Information regarding group testing is provided in Cook et al.[3] The behavior of grouted anchors arranged in groups or near edges is quite similar to the behavior of adhesive anchors described in this paper; however, the effects of a bond failure at the outer bond area between the grout and the concrete require a separate strength evaluation.

RESEARCH SIGNIFICANCE

The information provided in this paper represents the results of several years of numerical and experimental work performed in order to understand the behavior of adhesive bonded anchors when located in groups and/or near edges. As a result of this work, a behavioral model has been developed that can provide the basis for the design of these types of anchorages.

BACKGROUND

The design strength of anchorages to concrete is either controlled by the strength of the anchor steel or by the strength associated with the embedment of the anchors into the concrete. The design provisions regarding failure of the anchor steel in both tension and shear are provided in ACI 318-05, Appendix D,[1] and are applicable to adhesive and grouted anchors. The behavior of cast-in-place and post-installed mechanical anchors associated with embedment failure has been extensively studied[4,5] and embedment design provisions for these types of anchors are incorporated into ACI 318-05, Appendix D. Product approval standards for post-installed mechanical anchors are provided in ACI 355.2-04.[6] The embedment shear strength provisions of ACI 318-05, Appendix D, appear to be applicable to adhesive and grouted anchors; this will be addressed in a future paper.

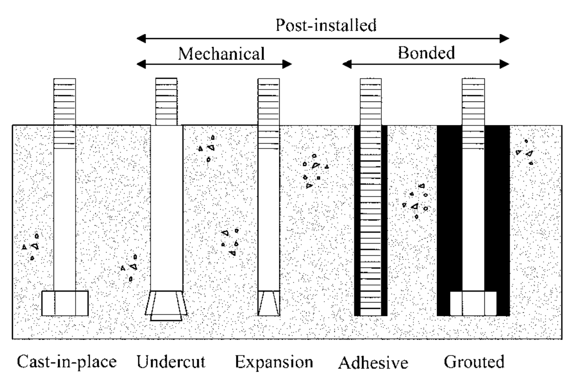

Fig. 1—Types of anchors.

ACI Structural Journal, V. 103, No. 6, November-December 2006.
MS No. 05-256 received September 17, 2005, and reviewed under Institute publication policies. Pertinent discussion including author's closure, if any, will be published in the September-October 2007 *ACI Structural Journal* if the discussion is received by May 1, 2007.

Rolf Eligehausen, *FACI, is Professor and Department Head for the Fastening Technology Department at the Institute of Construction Materials, University of Stuttgart, Stuttgart, Germany. He is a member of ACI Committees 349, Concrete Nuclear Structures; 355, Anchorage to Concrete; and 408, Bond and Development of Reinforcement.*

Ronald A. Cook, *FACI, is a Professor in the Civil Engineering Department at the University of Florida, Gainesville, Fla. He is Past Chair of ACI Committee 355, Anchorage to Concrete, and is a member of ACI Committees 318-B, Reinforcement and Development, and 349, Concrete Nuclear Structures.*

Jörg Appl *is a Doctoral Student in the Fastening Technology Department at the Institute of Construction Materials, University of Stuttgart.*

This paper is concerned with the behavior of adhesive bonded anchors loaded in tension and arranged in groups and/or with free edges near the anchors where the strength is limited by embedment failure.

The nominal bond strength of adhesive bonded anchors to be used in the design is dependent on the mean bond strength of anchors installed in accordance with manufacture guidelines, adjusted for scatter of the product test results, and for the product sensitivity to installation and in-service conditions. As discussed in Cook et al.[7] and Meszaros,[8] the bond strength of properly installed bonded anchor products varies quite considerably. Based on tests of 20 adhesive anchor products, Cook et al.[7] found that the mean bond strength at the adhesive/anchor interface for individual products ranged from 330 to 2830 psi (2.3 to 19.5 MPa). Results of tests performed by Meszaros[8] using three products indicated that the mean bond strength decreases as the anchor diameter increases.

In addition to the large variations in the mean bond strength for bonded anchors installed according to manufacture recommendations, each bonded anchor product is influenced differently by other conditions. These conditions include sensitivity to the hole cleaning procedure, hole drilling method (for example, hammer drilling or diamond core drilling), moisture presence in the concrete at installation, temperature effects, and creep under sustained loads. The implementation of the behavioral model presented in this paper is dependent on the acceptance of a comprehensive product evaluation standard that establishes a product nominal bond strength. ICC-ES AC-308[9] is a product evaluation standard accepted by the ICC Evaluation Service. Currently, ACI Committee 355 is developing a product evaluation standard that will be based on ICC-ES AC-308.[9]

The following provides the current information regarding the behavior of adhesive anchors loaded in tension in uncracked concrete. The effects of concrete cracks on the strength of cast-in-place and post-installed mechanical anchors is addressed in ACI 318-05, Appendix D. Information on the effects of concrete cracks on the strength of adhesive bonded anchors is provided in Eligehausen and Balogh[5] and Meszaros.[8] The information presented indicates that, on average, the bond strength is reduced by normal width cracks to approximately 50% of the value determined in uncracked concrete.

Cast-in-place and post-installed mechanical anchors

Fuchs et al.[4] proposed the behavioral model for concrete breakout failure currently incorporated into ACI 318-05, Appendix D. This model was created to predict the failure loads of cast-in-place headed anchors and post-installed mechanical anchors loaded in tension or in shear that exhibit concrete breakout failure. According to Fuchs et al.,[4] the mean concrete breakout capacity for single cast-in-place anchors and post-installed mechanical anchors in uncracked concrete is given by the following equations

Cast-in-place anchors

$$\bar{N}_b = 40\sqrt{f_c}h_{ef}^{1.5}\ \text{(lb)} \qquad \bar{N}_b = 16.8\sqrt{f_c}h_{ef}^{1.5}\ \text{(N)} \tag{1a}$$

Post-installed mechanical anchors

$$\bar{N}_b = 35\sqrt{f_c}h_{ef}^{1.5}\ \text{(lb)} \qquad \bar{N}_b = 14.7\sqrt{f_c}h_{ef}^{1.5}\ \text{(N)} \tag{1b}$$

It should be noted that the nominal concrete breakout strengths provided in ACI 318-05, Appendix D, are based on the 5% fractile using a coefficient of variation (COV) of 0.15 for cast-in-place anchors and 0.20 for post-installed mechanical anchors.

The concrete breakout capacity of anchor groups and anchors located near free edges with a tension load applied

Table 1(a)—Main parameters of tests in worldwide database: tests with anchor groups

		Concrete compressive strength f_c'		Diameter d		Embedment depth h_{ef}		Spacing s		h_{ef}/d		s/h_{ef}		s/d		$\bar{\tau}$	
		min.	max.	min.	max.	min.	max.	min.	max.							min.	max.
Type	Number of tests n	psi (MPa)	psi (MPa)	in. (mm)	in. (mm)	in. (mm)	in. (mm)	in. (mm)	in. (mm)	min.	max.	min.	max.	min.	max.	psi (MPa)	psi (MPa)
Group tests*	415	2320 (16.0)	7590 (52.3)	0.3 (8.0)	1.0 (24.0)	1.9 (48.0)	11.3 (288.0)	1.5 (38.1)	15.2 (384.0)	4.0	16.0	0.3	3.0	3.8	20.0	870 (6.0)	3050 (21.0)

*Groups with two and four anchors.

Table 1(b)—Main parameters of tests in worldwide database: tests with single anchors near edge

		Concrete compressive strength f_c'		Diameter d		Embedment depth h_{ef}		Edge distance c		h_{ef}/d		c/h_{ef}		c/d		$\bar{\tau}$	
		min.	max.	min.	max.	min.	max.	min.	max.							min.	max.
Type	Number of tests n	psi (MPa)	psi (MPa)	in. (mm)	in. (mm)	in. (mm)	in. (mm)	in. (mm)	in. (mm)	min.	max.	min.	max.	min.	max.	psi (MPa)	psi (MPa)
Edge tests*	133	3160 (21.8)	3860 (26.6)	0.3 (8.0)	1.0 (24.0)	3.0 (80.0)	12.3 (320.0)	1.2 (30.0)	9.5 (240.0)	7.8	20.0	0.3	1.5	3.0	20.0	1250 (8.6)	2600 (17.9)

*Single anchors.

concentrically to the anchors is given by Eq. (2) where $\overline{N}_b$ is taken from Eq. (1)

$$\overline{N}_{cb} = \frac{A_{Nc}}{A_{Nco}} \psi_{ed,N} \overline{N}_b \text{ (lb or N)} \quad (2a)$$

where

$$\psi_{ed,N} = 0.7 + 0.3\frac{c_{a1}}{c_{cr}} \text{ if } c_{a1} < c_{cr} \quad (2b)$$

Figure 2 provides information on how A_{Nco} and A_{Nc} are determined. According to ACI 318-05, Appendix D, for cast-in-place and post-installed mechanical anchors, the critical spacing s_{cr} is $3.0h_{ef}$ and the critical edge distance c_{cr} is $1.5h_{ef}$. Additional figures related to the evaluation of A_{Nc} are provided in ACI 318-05, Appendix D, as well as information if the anchors are not concentrically loaded in tension.

Single adhesive anchors

Figure 3 presents the embedment failure modes observed for single adhesive anchors. In Fig. 4, the transfer of load at the steel/mortar and mortar/concrete bond interfaces is shown. The mortar adhesive is the bonding agent used to connect the anchor with the concrete, either adhesive or grout. As shown in Fig. 4, a tension load is transferred by mechanical interlock from the threaded rod into the mortar and by adhesion and/or micro interlock (due to the roughness of the drilled hole) from the mortar into the concrete.

Experimental studies discussed in Eligehausen et al.,[10] indicate that the actual bond stress distribution along the embedment length at peak load is nonlinear with lower bond stresses at the concrete surface and higher bond stresses at the embedded end of the anchor. In Cook et al.,[11] however, a comparison of suggested behavioral models to a worldwide database for single adhesive anchors indicates that their failure load is best described by a uniform bond stress model incorporating the nominal anchor diameter d with the mean bond stress $\bar{\tau}$ associated with each product. This is confirmed by experimental and numerical studies of Meszaros[8] and McVay et al.[12] The uniform bond stress model for adhesive anchors is given by Eq. (3). This equation is valid for $4 \leq h_{ef}/d \leq 20$, $d \leq 2$ in. [50 mm], and a bond area $\pi d h_{ef} \leq 90$ in.^{2} [58,000 mm^2].

$$\overline{N}_\tau = \bar{\tau}\pi d h_{ef} \quad \text{(lb or N)} \quad (3)$$

According to Eligehausen et al.,[10] Zamora et al.,[2] and based on information presented in Cook et al.,[11] the failure load of single bonded anchors is limited by the concrete breakout failure load given by Eq. (1). This is shown in Fig. 5. In this figure, failure loads and failure modes of adhesive anchors with constant embedment depth but varying diameter are given. According to these test results, the failure load of adhesive anchors is limited to the concrete breakout failure load of post-installed mechanical anchors, as given by Eq. (1b). By equating Eq. (1b) with Eq. (3), the upper limit on the bond strength that can be used for single anchors can be determined (refer to Eq. (4))

$$\bar{\tau}_{max} = \frac{11.1 f_c^{0.5} h_{ef}^{0.5}}{d} \text{ (psi)} \quad (4a)$$

$$\bar{\tau}_{max} = \frac{4.7 f_c^{0.5} h_{ef}^{0.5}}{d} \text{ (MPa)} \quad (4b)$$

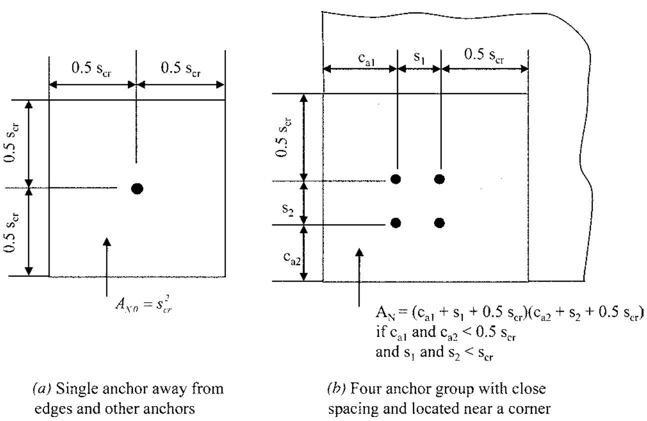

Fig. 2—Calculation of effective areas A_{Nco} and A_{Nc}.

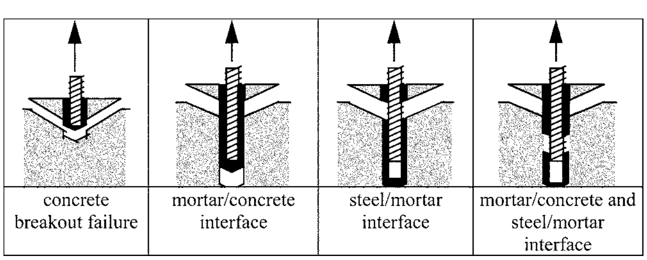

Fig. 3—Potential embedment failure modes of bonded anchors.[11]

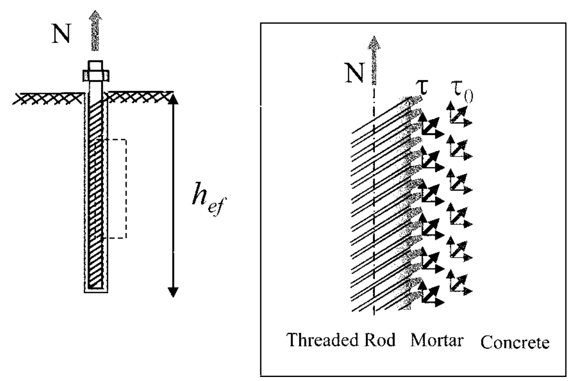

Fig. 4—Mechanism of load transfer of bonded anchor.[10]

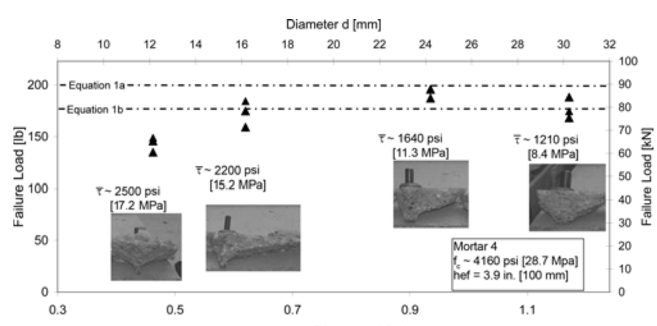

Fig. 5—Failure loads of single adhesive anchors as function of anchor diameter.[10]

NUMERICAL INVESTIGATION

To understand the behavior of adhesive anchors under tension loading, three-dimensional nonlinear finite element analyses were performed with the program developed by Ožbolt.[13] In this program, the concrete behavior is simulated by the microplane model described in detail in Ozbolt et al.[14] To assure objectivity of the results with respect to the size and orientation of the finite elements, the modified crack band method[14] was employed as a localization limiter. To avoid steel failure, elastic behavior of the anchor steel was assumed. The bond behavior of the mortar was modeled in different ways. In Meszaros[8] and Li et al.,[15,16] an interface model was used that only transfers shear stress. The shear strength is influenced by compression and tension stresses in the concrete perpendicular to the anchor. In recent studies performed at the University of Stuttgart,[17] the threads of the threaded rod were modeled and the mortar behavior was simulated using the microplane model with a proper calibration of the model parameters to represent the measured macroscopic mortar properties. The loading on the anchors was introduced under deformation control by applying incremental displacements to the anchor at the concrete surface.

Simulated single adhesive anchors were close to and far away from an edge as were quadruple anchor groups. Parameters varied for single anchors were anchor diameter, embedment depth, bond strength of the mortar, and edge distance. For anchor groups, the spacing of the anchors was also varied. In all numerical simulations, the concrete strength was 4300 psi (30 MPa) and the member thickness was large enough to avoid splitting failure. The chosen distance between anchors and the supports allowed the unrestricted formation of a concrete breakout cone.

Figure 6 shows the numerically obtained principal strains in concrete after passing peak load for a single anchor with a diameter d = 0.95 in. (24 mm) and a bond strength $\bar{\tau}$ = 1350 psi (9.3 MPa) as well as photographs of the anchors after tension tests. Figure 6(a_1) and (b_2) are for an anchor with $h_{ef}/d = 5$, while Fig. 6(a_2) and (b_2) are for $h_{ef}/d = 10$. Dark areas in Fig. 6(a_1) and (a_2) characterize crack formation.

With an embedment length of 5d, before reaching the peak load, short cracks begin to form along the embedment depth. Just prior to peak load, a crack forms at the base of the anchor, which grows with increasing imposed displacement resulting in a concrete breakout failure. For the case of the deeper embedment length shown in Fig. 6(a_2) and (b_2), a shallow cone is formed at the concrete surface and bond failure occurs along the remaining length of the anchor.

Figure 7 shows the principal tensile strains for a group of four adhesive anchors with d = 0.47 in. (12 mm), $h_{ef} = 10d$, and $\bar{\tau}$ = 1350 psi (9.3 MPa) after passing peak load. With a small spacing of $s = 4d$, a common concrete breakout cone starting at the base of the anchors is formed (Fig. 7(a)). With a larger spacing ($s = 8d$), the common concrete cone does not start at the base of the anchors but closer to the concrete surface. For a large spacing ($s = 16d$), the individual anchors of the group fail in the same way as single anchors with a pullout failure similar to that shown in Fig. 6(a_2) and (b_2). In Li et al.,[15] another potential failure mode (false pullout failure) is described, which is initiated by a horizontal crack at the base of the anchors followed by pullout of the individual anchors (Fig. 7(b_1) and (b_2)). This failure mode may occur at small to intermediate anchor spacings.

Figure 8 shows the numerically obtained failure loads of quadruple anchor groups with adhesive anchors (d = 0.47 in. [12 mm], $h_{ef} = 10d$) normalized by the failure load of single anchors as a function of the anchor spacing related to the anchor diameter (s/d). As with cast-in-place headed and post-installed mechanical anchors, the failure load of adhesive anchor groups increases with increasing spacing until they reach a limit of n times the single anchor strength at a critical spacing s_{cr}. Similarly, the failure load of anchorages with adhesive anchors located near edges decreases when the edge distance is smaller than a critical value c_{cr}. The failure load of anchorages with adhesive anchors can be modeled by Eq. (2); however, certain modifications are needed. They relate to the critical spacing, the critical edge distance, and the basic single anchor strength.

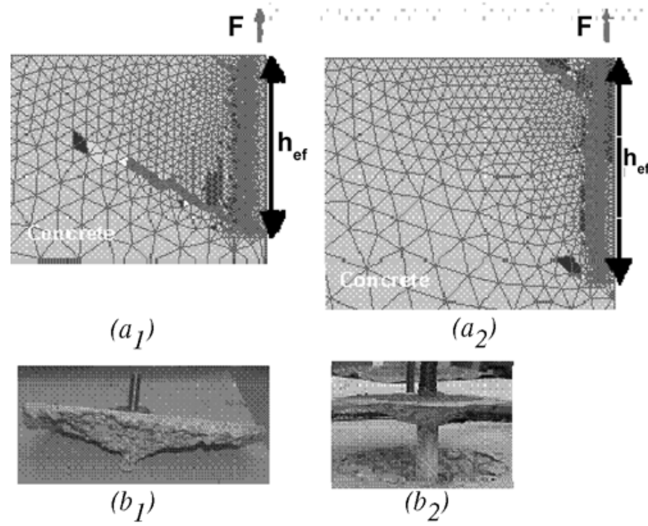

Fig. 6—(a) Failure modes of adhesive anchors, d *= 0.95 in. (24 mm) indicated by numerical modeling (dark areas characterize crack formation); and (b) test results. (a_1) and (b_1):* $h_{ef} = 5d$*; (a_2) and (b_2):* $h_{ef} = 10d$.

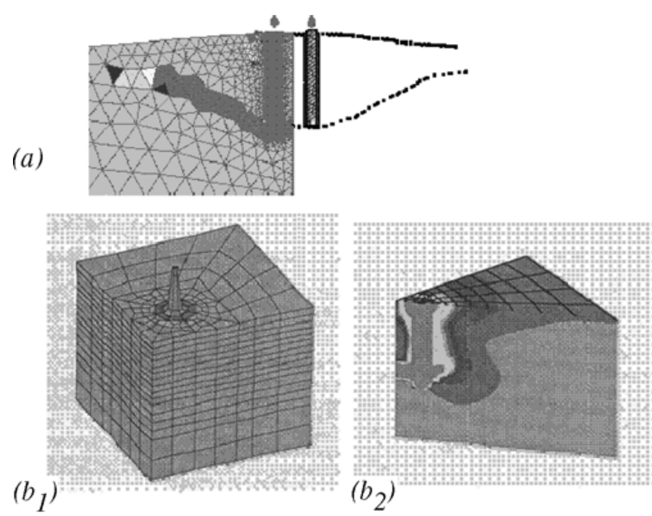

Fig. 7—(a) Failure mode of quadruple anchor group with adhesive anchors, d *= 0.47 in. (12 mm),* $h_{ef} = 10d$, $s = 4d$ *indicated by numerical modeling (dark areas characterize crack formation);[18] (b_1) deformed mesh at peak load (false pullout failure); and (b_2) principal strains at peak load indicating failure mode.[15]*

As indicated by Eq. (3), the bond strength $\bar{\tau}$, the anchor diameter d, and the anchor embedment length h_{ef} represent the parameters that could influence the critical spacing and critical edge distance. As a result of the numerical study by Li et al.,[15] it was determined that the critical spacing is not significantly influenced by the embedment depth h_{ef} of the anchors. This is shown in Fig. 9 where the ratios between the numerically obtained failure loads for anchor groups to the failure load of single anchors with the same embedment depth are plotted as a function of the anchor spacing. The only parameter varied in Fig. 9 is the embedment depth h_{ef}. If the critical spacing were influenced by the embedment depth, groups with smaller embedment depths would reach the capacity of four single anchors at smaller spacings than those with larger embedment depths. For a given spacing, however, the related failure load is nearly independent of the embedment depth. This behavior can be explained by Fig. 10, which shows that the width of the principal compression stress field of single anchors with significantly different embedment lengths is nearly identical. The width of the compression stress field is directly related to the critical spacing.

Li et al.[15] found that the critical spacing is dependent on anchor diameter d. This can be seen in Fig. 11, which shows related failure loads of groups of anchors with different diameters as a function of the spacing related to the anchor diameter (s/d). The related group failure load is almost independent of the anchor diameter for a constant ratio of s/d and reaches the full capacity of four individual anchors at approximately the same value of s/d.

Studies by Li and Eligehausen[16] indicated that the critical spacing is also influenced by bond strength $\bar{\tau}$. In Fig. 12, the ratio of the anchor group strength to the single anchor strength is plotted as a function of the anchor spacing. In the numerical calculations, the anchor diameter and embedment depth were held constant and the bond strength was varied. For anchorages with the highest bond strength, failure occurred by concrete breakout. Therefore, and as a result, the assumed bond strength was not fully used. The conclusion that the critical spacing is influenced by bond strength is confirmed by Fig. 13, which shows that the width of the principal compression stress field of a single anchor with constant embedment depth increases with increased bond strength.

To determine the critical spacing s_{cr}, a large numerical parametric study with anchor groups was performed at the University of Stuttgart.[18] The parameters varied included anchor diameter, embedment depth, concrete strength, bond strength, and anchor spacing. In each individual numerical test series, the anchor diameter, embedment depth, and bond strength were kept constant and the anchor spacing was

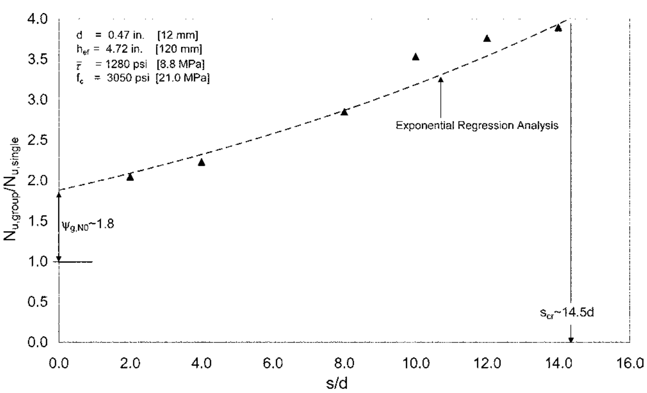

Fig. 8—Numerically obtained failure loads of quadruple groups related to failure load of single anchor as function of ratio of spacing to anchor diameter.[18]

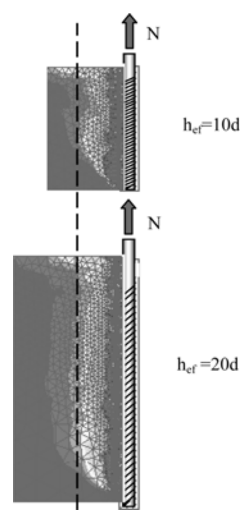

Fig. 10—Principal compression stresses in concrete. Single adhesive anchors d *= 0.47 in. (12 mm).*[18]

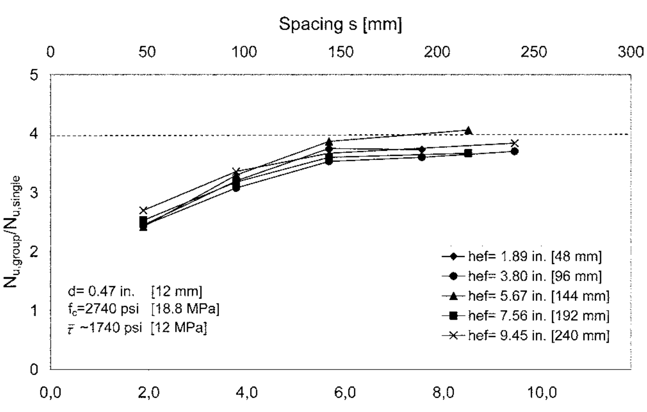

Fig. 9—Numerically obtained failure loads of quadruple groups with adhesive anchors related to failure load of single anchor as function of anchor spacing. Parameter is embedment depth.[15]

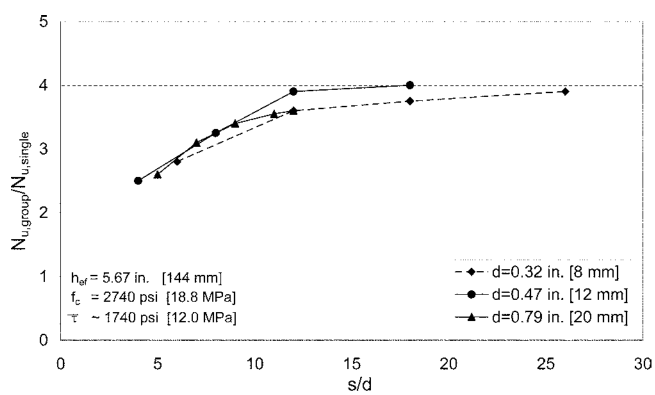

Fig. 11—Numerically obtained failure loads of quadruple groups with adhesive anchors related to failure load of single anchor as function of ratio anchor spacing to diameter. Parameter is anchor diameter.[15]

varied. For each individual numerical test series, the critical spacing was evaluated, as shown in Fig. 8. The relationship between the numerically obtained group failure loads and the spacing was approximated by an exponential function, which was found by regression analysis. The critical spacing was determined by extrapolating this function to the value of $N_{u,group}/N_{u,single} = 4$. Figure 14 provides a summary of the results. The values of the critical spacing found from each test series divided by the diameter (s_{cr}/d) are plotted as a function of the bond strength. The critical spacing s_{cr} resulting from the numerical analysis is best described by Eq. (5). The critical edge distance c_{cr} may be taken as one half of the critical spacing.

$$s_{cr} = 2c_{cr} = 14.7d\left(\frac{\bar{\tau}}{1450}\right)(\text{in.}) \tag{5a}$$

$$s_{cr} = 2c_{cr} = 14.7d\left(\frac{\bar{\tau}}{10}\right)(\text{mm}) \tag{5b}$$

Based on the aforementioned considerations, the failure load of adhesive anchor groups and/or anchorages located near edges can be calculated by Eq. (2) with N_b replaced by N_τ from Eq. (3) and using s_{cr} and c_{cr} determined from Eq. (5). However, a further aspect related to anchorages with adhesive anchors should be accounted for.

In the case of concrete cone failure, the failure load of a group of anchors with a theoretical spacing of $s = 0$ is equal to the value valid for a single anchor (refer to Eq. (2)). When extrapolating the regression lines that describe the failure loads for bonded anchor groups to a spacing of $s = 0$, however, the group failure load is larger than that of a single anchor (refer to Fig. 8, 9, 11, and 12). This increase is denoted by the factor $\psi_{g,No}$ in Fig. 8. It is explained in Fig. 15. If the bond strength is low, the failure of two adjacent anchors is caused by bond failure resulting in anchor pullout. The bond failure area of the two adjacent anchors is approximately equal to $\sqrt{n}$ times the effective bond area of a single anchor. Therefore, the failure load of the group is $\sqrt{n}$ times the failure load of a single anchor ($\psi_{g,No} = \sqrt{n}$). In contrast, the failure load of a group of adjacent anchors is not increased over that of a single anchor when failure is controlled by concrete breakout ($\psi_{g,No} = 1$). The value of $\psi_{g,No}$ should be related to the bond strength. If the bond strength is equal to $\bar{\tau}_{max}$ according to Eq. (4), then a single anchor will fail by concrete breakout and $\psi_{g,No} = 1.0$. If the bond strength is very small (for example, $\bar{\tau} < 0.3\bar{\tau}_{max}$), then failure of the group will be caused by anchor pullout resulting in $\psi_{g,No} \approx \sqrt{n}$. Values for $\psi_{g,No}$ between these limiting cases were

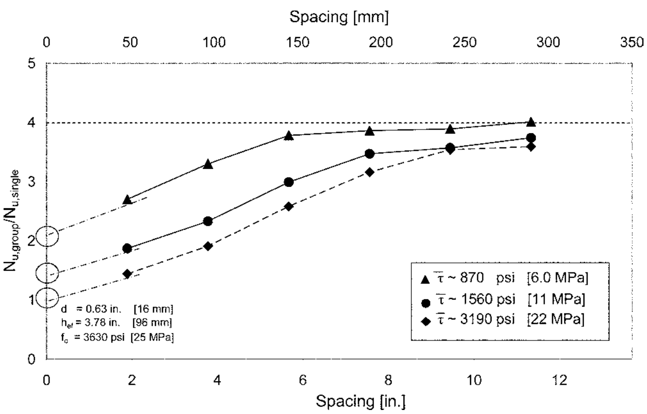

Fig. 12—Numerically obtained failure loads of quadruple groups related to failure load of single anchor as function of anchor spacing. Parameter is mean bond strength of single anchors.[16]

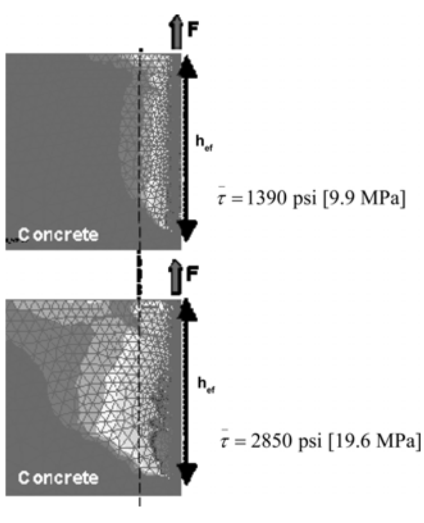

Fig. 13—Principal compression stresses in concrete. Single adhesive anchor, d *= 0.95 in. (24 mm),* h_{ef} *= 20*d.[18]

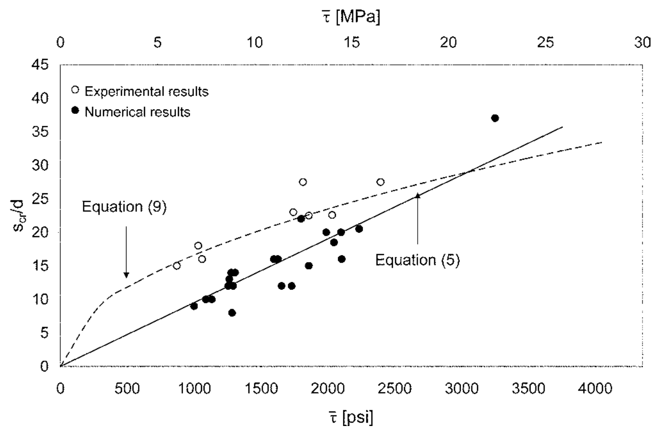

Fig. 14—Related critical spacing s_{cr}/d *as a function of mean bond strength* $\bar{\tau}$.

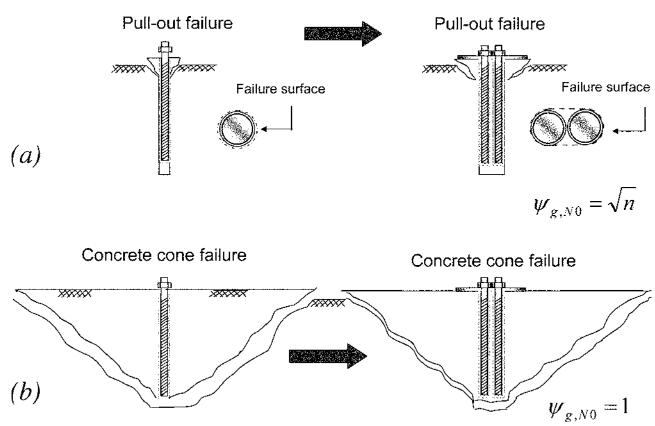

Fig. 15—Increase of failure area and failure load for: (a) pullout failure; and (b) concrete cone failure.[17]

determined from the results of the individual numerical test series of quadruple anchor groups as shown in Fig. 8. They are plotted in Fig. 16 as a function of the ratio $\bar{\tau}/\bar{\tau}_{max}$ and can be approximated by Eq. (6).

$$\psi_{g,No} = \sqrt{n} - (\sqrt{n} - 1)\left(\frac{\bar{\tau}}{\bar{\tau}_{max}}\right)^{1.5} \geq 1.0 \tag{6}$$

The influence of the increase in bond area on the failure load decreases with increasing spacing. This effect is taken into account by a factor $\psi_{g,N}$. It is assumed that this factor linearly decreases between $s = 0$ where $\psi_{g,N} = \psi_{g,No}$ and $s = s_{cr}$ where $\psi_{g,N} = 1.0$. This leads to Eq. (7).

$$\psi_{g,No} = \psi_{g,No} - \frac{s}{s_{cr}}(\psi_{g,No} - 1) \tag{7}$$

Taking the aforementioned considerations into account, the mean failure load of anchorages using adhesive anchors may be calculated as follows

$$\bar{N}_T = \frac{A_{Nc}}{A_{Nco}}\psi_{ed,N}\psi_{g,N}\bar{N}_\tau \leq \bar{N}_{cb} \text{ (lb or N)} \tag{8}$$

In Eq. (8), A_{Nc} and A_{No} are determined according to Fig. (2), $\psi_{ed,N}$ is given by Eq. (2b), $\psi_{g,N}$ is given by Eq. (7), and $\bar{N}_\tau$ is determined from Eq. (3). The critical spacing s_{cr} and critical edge distance c_{cr} provided by Eq. (5) should be used when calculating A_{Nc} and A_{No}, $\psi_{ed,N}$ and $\psi_{g,N}$. In all numerical simulations, the calculated failure load of anchorages with adhesive anchors was smaller than the numerically obtained failure load of the same anchorages with headed anchors. Therefore, in Eq. (8), the mean bond failure load $\bar{N}_{cb}$ is limited to the mean concrete breakout failure load $\bar{N}_b$, given by Eq. (2) using $\bar{N}_b$ according to Eq. (1b) for post-installed mechanical anchors.

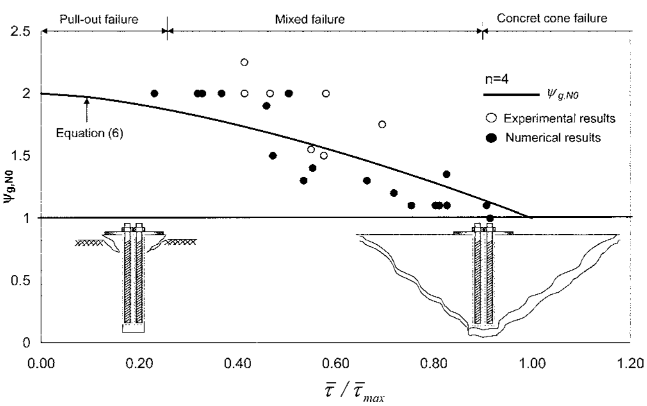

Fig. 16—Factor $\psi_{g,N0}$ as function of mean bond strength $\bar{\tau}$ related to maximum value $\bar{\tau}_{max}$ according to Eq. (4).[17]

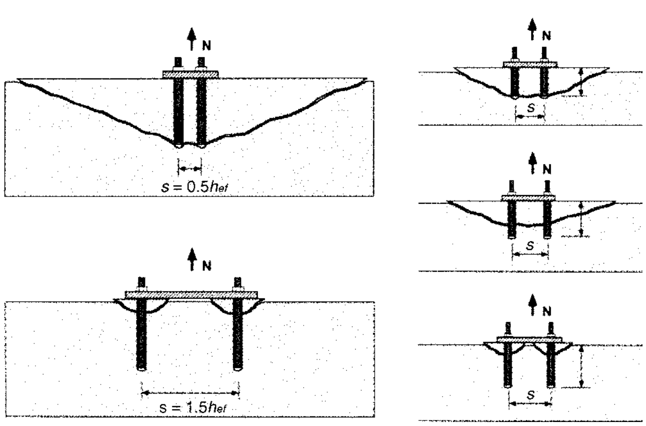

Fig. 17—Failure modes of groups of adhesive anchors observed in tests.[19]

EXPERIMENTAL INVESTIGATION

A worldwide database was compiled based on experimental investigations with adhesive anchors arranged in groups or located near free edges. It is based on that presented by Lehr;[19] however, tests by Appl[17] were added that were performed after Lehr's work was completed. The database used for this study includes the results of 353 group tests with four anchors, 62 group tests with two anchors, and 133 tests with single anchors located near a free edge. For comparison to the group and edge tests, the database also includes baseline single anchor tests that were performed away from free edges with the same size anchors, adhesive anchor product, and concrete as used in the anchor group or edge tests. In all tests in the database, the distance between the reaction frame and the anchors was large enough to allow the formations of an unrestricted concrete breakout cone. Failure occurred in all tests by bond failure or breakout of a concrete cone. Table 1 provides a summary of the critical parameters that were included in these 548 group and edge tests.

Figure 17 shows the types of failures observed during the testing of quadruple groups of adhesive anchors. In the two figures shown on the left side of Fig. 17, the embedment depth was kept constant and the anchor spacing was increased. The failure mode changed from a concrete breakout starting at the base of the anchors to a pullout failure with a shallow cone at a large spacing. The three figures shown on the right side of Fig. 17 are valid for anchor groups with a ratio $s/h_{ef} = 1$, but increasing embedment depth. The failure mode changes from a concrete breakout starting at the base of the anchors over a common partial concrete cone to an individual anchor pullout with shallow cones at the surface. The change in failure mode occurs because the load that can be introduced by bond into the concrete increases linearly with h_{ef} while the concrete breakout strength increases in proportion to $h_{ef}^{1.5}$. Note that the numerically obtained failure modes agree with those observed in the experiments.

Figure 18 depicts the results of an example test series of anchor groups where the anchor spacing s was varied while the anchor diameter d, bond strength τ_u, and embedment depth h_{ef} were held constant. The failure load of the anchor group increases with increased spacing but is much lower than the concrete breakout failure load given by Eq. (2). From the results of test series in which only the anchor spacing was varied, the critical spacing s_{cr} and the factor $\psi_{g,No}$ were determined, as shown in Fig. 8. The experimentally obtained values for $\psi_{g,No}$ agree sufficiently well with those obtained from the results of the numerical analysis (refer to Fig. 16). However, the critical spacings s_{cr} evaluated from the experimental results differ from those obtained numerically (refer to Fig. 14). Based on the experimental results, the critical spacing s_{cr} can be approximated by Eq. (9).

Table 2—Comparison of measured failure loads with predicted values

Type	Pullout failure predicted			Concrete breakout failure predicted			Pullout and concrete breakout failure		
	No. of tests	Mean N_{test}/N_{pred}	COV, %	No. of tests	Mean N_{test}/N_{pred}	COV, %	No. of tests	Mean N_{test}/N_{pred}	COV, %
Group tests with two and four anchors	377	0.98	15.1	38	1.05	16.3	415	0.99	15.4
Group tests with two and four anchors but without $\psi_{g,N}$	392	1.21	18.3	23	1.04	16.9	415	1.20	18.5
Single anchor edge tests	133	1.30	19.6	—	—	—	133	1.30	19.6

$$s_{cr} = 2c_{cr} = 20d\left(\frac{\bar{\tau}}{1450}\right)^{0.5}\text{(in.)} \tag{9a}$$

$$s_{cr} = 2c_{cr} = 20d\left(\frac{\bar{\tau}}{10}\right)^{0.5}\text{(mm)} \tag{9b}$$

BEHAVIORAL MODEL

As a result of numerical and experimental work, a behavioral model was developed that best describes the failure loads of anchorages with adhesive anchors where the effects of anchor groups and/or edges needs to be accounted for. The behavioral model incorporates both the potential concrete breakout failure mode and potential pullout failure mode.

The behavioral model is provided by Eq. (8); however, the critical spacing s_{cr} and critical edge distance c_{cr} provided by Eq. (9) should be used when calculating A_{Nc} and A_{No} according to Fig. 2, $\psi_{ed,N}$ according to Eq. (2b), and $\psi_{g,N}$ according to Eq. (7).

For design, appropriate capacity reduction factors and nominal strengths must be addressed in developing code provisions to implement the findings of this research. It is suggested that the 5% fractile of the bond strength be used for the design of bonded anchors, which should be adjusted to consider several influencing factors on anchor performance such as sensitivity to hole cleaning procedures and increased temperature as well as long term behavior.

COMPARISON OF BEHAVIORAL MODEL WITH EXPERIMENTAL RESULTS

In Fig. 19 and 20, the ratios of the measured failure loads divided by the strengths predicted by the behavioral model (N_{test}/N_{pred}) are plotted as a function of several parameters varied in the tests. Figure 19 and 20 also show the best fit trend lines. If these lines are horizontal and are located at N_{test}/N_{pred} = 1.0, then the influence of the varied parameter on the failure load is well taken into account by the behavioral model. Table 2 provides a statistical evaluation of the ratios N_{test}/N_{pred}.

As indicated by Fig. 19, the behavioral model provides an excellent fit to the experimental results with groups. For the 415 tests, the mean value of N_{test}/N_{pred} is 0.99 with a COV of 15.4%. An equally good prediction is obtained when the data are separated into tests where the calculated pullout failure or concrete breakout failure controls the calculated resistance (Table 2). In summary, the proposed behavior model for groups with adhesive anchors is as accurate as the behavior model for headed anchors. An equally good fit is provided to the individual group test series, as shown by the example in Fig. 18. As shown in Fig. 20 and Table 2, however, the predicted failure loads are conservative for anchorages located very near to a free edge.

The proposed behavioral model for adhesive anchors (Eq. (8)) is very similar to the behavioral model for headed anchors (Eq. (2)) except for the $\psi_{g,N}$ factor in Eq. (8). Therefore, for reasons of simplification, it might be tempting to neglect

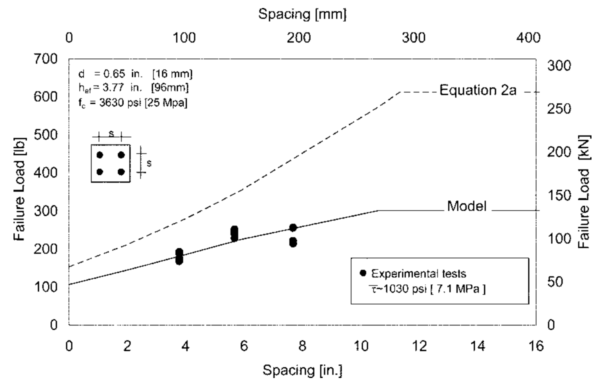

Fig. 18—Comparison of measured and predicted failure loads of groups of adhesive anchors as function of spacing.

this factor. Figure 21 provides the same type of information as Fig. 19; however, the $\psi_{g,N}$ factor is not incorporated in the behavioral model. As shown in Fig. 21, the behavioral model neglecting $\psi_{g,N}$ does not provide the excellent fit exhibited when this factor is included and is rather conservative for groups with a small spacing.

SUMMARY AND CONCLUSIONS

Based on the results of both numerical and experimental investigations, a behavioral model to predict the average failure load of anchorages using adhesive bonded anchors is proposed. The model is similar to the behavioral model that predicts the concrete breakout failure load of cast-in-place and post-installed mechanical anchors incorporated in ACI 318-05, Appendix D, but with the following modifications.

The basic strength of a single adhesive anchor predicts the pullout capacity and not the concrete breakout capacity. It is based on the uniform bond stress model, as given by Eq. (3). The critical spacing and critical edge distance of adhesive anchorages depend on the anchor diameter and the bond strength and not on the anchor embedment depth. Furthermore, an additional factor $\psi_{g,N}$ is used that takes into account the larger bond area of closely spaced adhesive anchors in comparison to a single anchor. The failure load of anchorages with adhesive anchors is limited to the concrete cone failure load of post-installed mechanical anchors.

The proposed behavioral model agrees very well with the results of 415 group tests contained in a worldwide database. Based on a comparison to 133 tests with single anchors close to an edge, the behavioral model is conservative for anchorages located very near to an edge.

ACKNOWLEDGMENTS

The authors wish to express their gratitude and sincere appreciation to the manufacturers and individuals contributing to the extensive numerical and experimental work presented in this paper. Sponsoring manufacturers were fischerwerke, Hilti AG, and Würth KG. P. Pusill-Wachtsmuth of Hilti AG and R. Mallée of fischerwerke deserve special recognition for their contributions over the years. B. Lehr, J. Meszaros, and H. Spieth all deserve credit for their results presented in this paper.

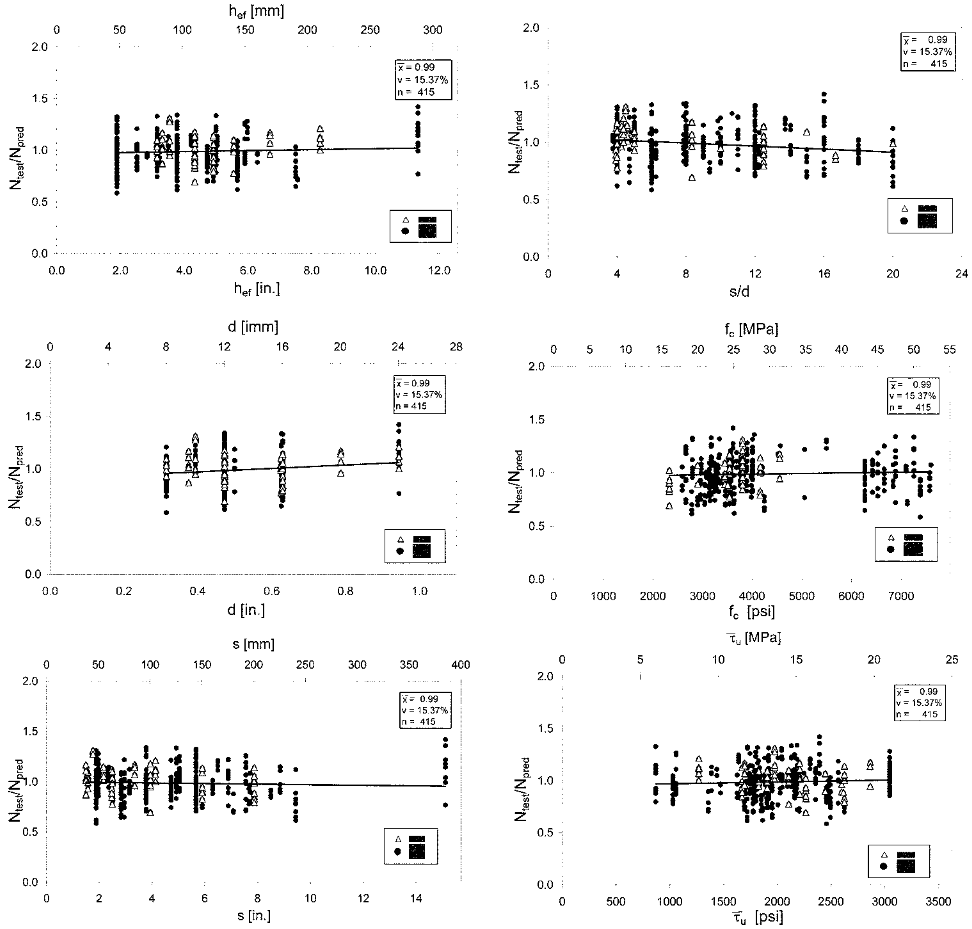

Fig. 19—Measured failure loads of anchor groups compared with predicted results plotted against h_{ef}, s/d, d, f_c, s, *and* $\bar{\tau}$.

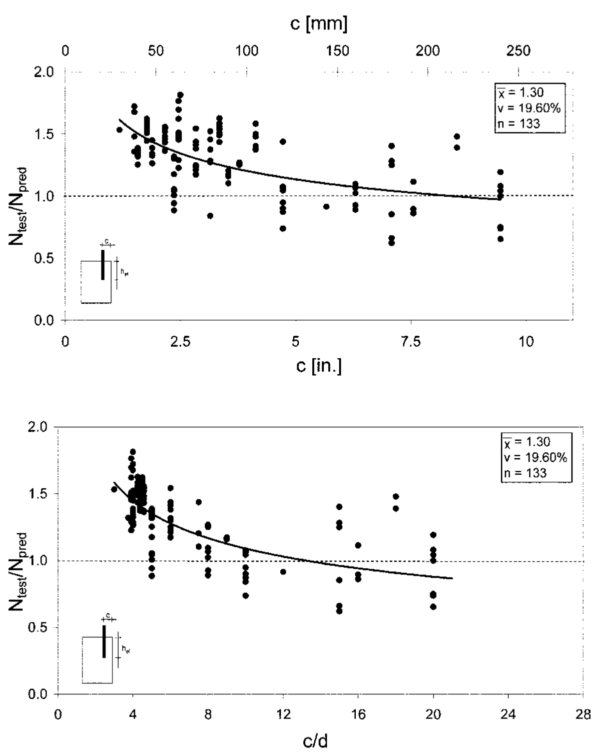

Fig. 20—Measured failure loads of single anchors near to edge compared with predicted results plotted against edge distance c *and ratio* c/d.

NOTATION

A_{Nc} = projected concrete failure area of single anchor or group of anchors for calculation of strength in tension, in.^{2} (mm^2)
A_{Nco} = projected concrete failure area of single anchor for calculation of strength in tension if not limited by edge distance or spacing, in.^{2} (mm^2)
c_{cr} = edge distance where strength of anchor is not influenced by free edge, in. (mm)
d = diameter of anchor, in. (mm)
d_o = diameter of hole, in. (mm)
f_c = compressive strength of concrete, psi (MPa)
h_{ef} = effective embedment depth of anchor, in. (mm)
$\bar{N}_b$ = mean basic concrete breakout strength in tension of single anchor in uncracked concrete, lb (N)
$\bar{N}_{cb}$ = mean concrete breakout strength in tension of single anchor at edge or of group of anchors in uncracked concrete, lb (N)
$\bar{N}_T$ = mean bond pullout strength in tension of single adhesive anchor at edge or of group of adhesive anchors in uncracked concrete, lb (N)
$\bar{N}_\tau$ = mean bond pullout strength in tension of single adhesive anchor in uncracked concrete, lb (N)
$\frac{N_{test}}{N_{pred}}$ = ratio of actual test results to predicted results
s_{cr} = anchor spacing where anchor strength is not influenced by other anchors, in. (mm)
$\bar{\tau}$ = mean uniform bond strength at steel/mortar interface, psi (MPa)
$\bar{\tau}_{max}$ = maximum mean uniform bond strength at steel/mortar $\psi_{ed,N}$ = factor used to modify tensile strength of anchors based on proximity to edges of concrete member
$\psi_{g,N}$ = factor used to modify tensile strength of adhesive anchors based on number and spacing of anchors in group and mean bond strength
$\psi_{g,No}$ = factor used with $\psi_{g,N}$ to modify tensile strength of adhesive anchors based on number of anchors in group and mean bond strength

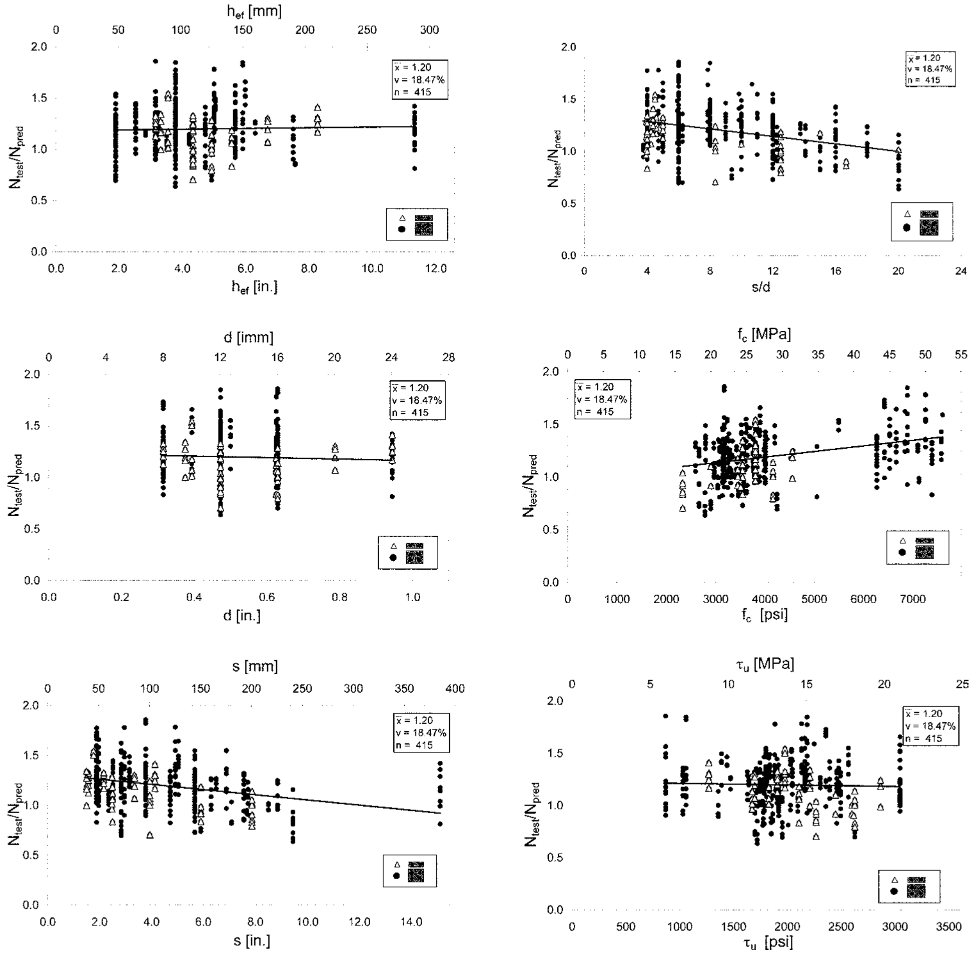

Fig. 21—Measured failure loads of anchor groups compared with predicted results neglecting factor $\psi_{g,N}$ plotted against h_{ef}, s/d, d, f_c, s, *and* $\bar{\tau}$.

REFERENCES

1. ACI Committee 318, "Building Code Requirements for Structural Concrete (ACI 318-05) and Commentary (318R-05)," American Concrete Institute, Farmington Hills, Mich., 2005, 430 pp.

2. Zamora, N. A.; Cook, R. A.; Konz, R. C.; and Consolazio, G. R., "Behavior and Design of Single, Headed, and Unheaded Grouted Anchors under Tensile Load," *ACI Structural Journal*, V. 100, No. 2, Mar.-Apr. 2003, pp. 222-230.

3. Cook, R. A.; Burtz, J. L.; and Ansley, M. H., "Design Guidelines and Specifications for Engineered Grouts," *FDOT Research Report* BC354 RPWO, No. 48, Aug. 2003, available at http://www.dot.state.fl.us/research-center/Completed_Structures.htm.

4. Fuchs, W.; Eligehausen, R.; and Breen, J. E., "Concrete Capacity Design (CCD) Approach for Fastening to Concrete," *ACI Structural Journal*, V. 92, No. 1, Jan.-Feb. 1995, pp. 73-94.

5. Eligehausen, R., and Balogh, T., "Behavior of Fasteners Loaded in Tension in Cracked Reinforced Concrete," *ACI Structural Journal*, V. 92, No. 3, May-June 1995, pp. 365-379.

6. ACI Committee 355, "Qualification of Post-Installed Mechanical Anchors in Concrete and Commentary (ACI 355.2-04/355.2R-04)," American Concrete Institute, Farmington Hills, Mich., 2004, 31 pp.

7. Cook, R. A., and Konz, R. C., "Factors Influencing Bond Strength of Adhesive Anchors," *ACI Structural Journal*, V. 98, No. 1, Jan.-Feb. 2001, pp. 76-86.

8. Meszaros, J., "Tragverhalten von Verbunddübeln im ungerissenen und gerissenen Beton," Doctoral thesis, University of Stuttgart, Stuttgart, Germany, 1999. (in German)

9. ICC-ES AC-308, "Acceptance Criteria for Post-Installed Adhesive Anchors in Concrete," ICC Evaluation Services, Inc., Whittier, Calif., 2005.

10. Eligehausen, R.; Appl, J. J.; Lehr, B.; Meszaros, J.; and Fuchs, W., "Tragverhalten und Bemessung von Befestigungen mit Verbunddübeln unter Zugbeanspruchung, Part 1: Einzeldübel mit großem Achs-und Randabstand," Beton und Stahlbetonbau 99, No. 7, July 2004, pp. 561-571. (in German)

11. Cook, R. A.; Kunz, J.; Fuchs, W.; and Konz, R. C., "Behavior and Design of Single Adhesive Anchors under Tensile Load in Uncracked Concrete," *ACI Structural Journal*, V. 95, No. 1, Jan.-Feb. 1998, pp. 9-26.

12. McVay, M.; Cook, R. A.; and Krishnamurthy, K., "Pullout Simulation of Post-Installed Chemically Bonded Anchors," *Journal of Structural Engineering*, ASCE, V. 122, No. 9, Sept. 1996, pp. 1016-1024.

13. Ožbolt, J., "MASA-Finite Element Program for Nonlinear Analysis of Concrete and Reinforced Concrete Structures," *Research Report*, Institute of Construction Materials, University of Stuttgart, Stuttgart, Germany, 1998, 74 pp.

14. Ožbolt, J.; Li, Y.-J.; and Kozar, I., "Microplane Model for Concrete with Relaxed Kinematic Constraint," *International Journal of Solids and Structures*, V. 38, 2001, pp. 2683-2711.

15. Li, Y.-J.; Eligehausen, R.; Ožbolt, J.; and Lehr, B., "Numerical Analysis of Quadruple Fastenings with Bonded Anchors," *ACI Structural Journal*, V. 99, No. 2, Mar.-Apr. 2002, pp. 149-156.

16. Li, Y.-J., and Eligehausen, R., "Numerical Analysis of Group Effect of Bonded Anchors with Different Bond Strengths," *Connections between Steel and Concrete*, RILEM Proceedings PRO 21, RILEM Publications, 2001, pp. 699-707, available at http://www.rilem.net/pro21.php.

17. Appl, J., and Eligehausen, R., "Gruppenbefestigungen mit Verbunddübeln—Bemessungskonzept," *Report* No. 03/27-2/55, Institute of Construction Materials, University of Stuttgart, Stuttgart, Germany, 2003. (in German)

18. Appl, J., and Eligehausen, R., "Gruppenbefestigungen mit Verbunddübeln—Numerische Untersuchung," *Report* No. 05/07-2/66, Institute of Construction Materials, University of Stuttgart, Stuttgart, Germany, 2005. (in German)

19. Lehr, R., "Tragverhalten von Verbunddübeln im ungerissenen unter zentrischer Belastung im ungerissenen Beton—Gruppenbefestigungen und Befestigungen am Bauteilrand,"Doctoral thesis, University of Stuttgart, Stuttgart, Germany, 2003. (in German)

Disc. 103-S79/From the Nov.-Dec. 2006 *ACI Structural Journal*, p. 783

Strain-Based Shear Strength Model for Slender Beams without Web Reinforcement. Paper by Hong-Gun Park, Kyoung-Kyu Choi, and James K. Wight

Discussion by Himat Solanki

PE, Building Department, Sarasota County Government, Sarasota, Fla.

The authors have presented an interesting concept on shear strength of slender beams without web reinforcement. The discusser would like to offer the following:

1. There are some inconsistencies involved in the $\bar{\sigma}$ value. Based on the Kato study,[55] the average ratio of $\bar{\sigma}/f_c'$ equals 0.142, which is consistent in Mphone[29] beams (a lower f_c' value resulted in a higher ratio $\bar{\sigma}/f_c'$, whereas a higher f_c' value resulted in a lower ratio $\bar{\sigma}/f_c'$). The condition does not exist in the Ahmad and Lue[30] and Leonhardt and Walther[7] beams.

For example, the Mphonde[29] Beam A0-33-C versus the Leonhardt and Walther[7] Beam 5*r*: alhough the Leonhardt and Walther[7] beams have a low reinforcement ratio, approximately 50% of the Mphonde beam, the $\bar{\sigma}$ value is much higher than the Mphonde beams. Also, when a ratio of $\bar{\sigma}/f_c'$ was compared for Beam 5*r* versus Beam A0-33-C, a significant inconsistency was noted between these two beams.

To further thoroughly review all three Ahmad and Lue[30] beams, the following inconsistencies were noted.

In Beam A8, f_c' = 9.6 ksi and ρ = 1.45% with $\bar{\sigma}/f_c'$ = 0.202, whereas in Beam A2, f_c' = 9.6 ksi and ρ = 3.14% with $\bar{\sigma}/f_c'$ = 0.175, that is, a 15% lower value of $\bar{\sigma}/f_c'$ than Beam A8, even though ρ is 216% greater than that of Beam A8.

Beam C2 has f_c' = 10.1 ksi and ρ = 4.81 with $\bar{\sigma}/f_c'$ = 0.1802, which is a 4% higher value of $\bar{\sigma}/f_c'$ than Beam A2 but a 12% lower value of $\bar{\sigma}/f_c'$ than Beam A8. It was also noted in the Ahmad and Lue Beam A8 versus Leonhardt and Walther Beam 5*r*.

2. It was noted in Fig. 10 that the authors' proposed method (Fig. 10(a)) does not significantly depart from Okamura and Higai[11] (Fig. 10(c)) and Kim and Park[23] (Fig. 10(g)). The Okamura and Higai[11] equation, however, has some limitation such as the *a*/*d* ratio and the longitudinal reinforcement ratio ρ. Also, Kim and Park[23] have certain limitations such as a power of compressive strength ($[(f_c')^{\alpha}]\alpha$ cited in the original paper), the *a*/*d* ratio, and depth of beam *d*. Based on these limitations in both equations, numerous beams out of 400 beams specified in Table 3, as well as approximately 50% of the beams as specified in Table 2, would not qualify for the Okamura and Higai[11] and/or Kim and Park[23] equations, depending upon their limitations.

Because the Kim and Park[23] equation is similar to the Kennedy[56] equation, and because the Okamura and Hagai[11] equation is similar to the Hedman-Losberg[57] equation, the authors should have considered these two equations in their Fig. 10 and possibly eliminated Zararis and Papadakis,[15] Bažant and Sun,[13] and/or CSA.[24]

The Kennedy equation[56] (based on over 500 test specimens) is

$$v_c = 0.312 f_c'^{\,0.426} d^{-0.282}[1 + (\{M/Vd\}/0.25\rho)]$$

The Hedman-Losberg equation[57] (based on over 1000 test specimens) is

$$v_c = 0.09(1.75 - 1.25d)(1 + 50\rho)\sqrt{f_c'}$$

where $1.75 - 1.25d \geq 1.0$ and $\rho \leq 0.02$.

3. The C_{x1} or C_a value varies from 0.25*d* to 0.5*d*, depending upon the amount of longitudinal reinforcement and the plasticity of concrete. Based on the authors' stress-strain diagrams, no consideration was given to the plasticity in the concrete.[58] The plasticity has a significant impact on the ratio of depth of compression force to the effective depth of the beams.

Tanaka and Kishi[59] have proposed the following simplified expression. From Fig. 6, the depth of compression zone is

$$c_{x1} = c_a - \int_{x_0}^{a} \tan\theta(x, z)\,dx$$

where $\tan\theta = jd/a$ and x and z equal the longitudinal and vertical axes, respectively.

Based on the test data, $C_{x1} = kC_a$; $k = \beta_1(e^{\beta_2 x_0} - e^{-\beta_2 x_0})$; $\beta_1 = 0.103 f_c'^{\,-0.08} \cdot \rho^{0.28}$; $\beta_2 = 2.31 f_c'^{\,0.03} \cdot \rho^{-0.09}$; and x_0 = 1.0 – 0.11*a*/*d* when $a/d \leq 2.7$ and 0.7 when $a/d \geq 2.7$

4. Because the Ahmad and Lue[30] and Leonhardt and Walther[7] beams depart from the Mphonde[29] beams in Table 2, the discusser has revisited and re-evaluated those beams. The results are shown in Table A. The analytical values of $\bar{\sigma}$ are very consistent with Kato,[55] and the v_{pred} is in very good agreement with test results.

5. The discusser has not analyzed all the beams as outlined in Table 3 due to the unavailability of some of test specimens[41] and the brevity of the discussion. Based on Table A and some of the observations made by the discusser (flexural strength of concrete, σ or σ_u, [Eq. (14), (15), and (18)], and the neutral axis of the beams) and Fig. 10(a) through (h), the discusser believes that the authors' proposed method needs significant further improvement/refinement.

Table A—Dimensions and properties of Ahmad and Lue's[30] and Leonhardt and Walther's[7] specimens, and strength predictions

Specimens		f_c', ksi	$\bar{\sigma}$	v_{exp}, ksi	v_{pred}, ksi
Ahmad and Lue[30]	A8	9.6	1.36	0.27	0.28
	A2	9.6	1.50	0.39	0.37
	C2	10.1	1.58	0.47	0.47
Leonhardt and Walther[7]	5*r*	4.1	0.64	0.22	0.22
	6*r*	4.1	0.64	0.20	0.21
	7-2	4.3	0.67	0.19	0.20
	8-2	4.3	0.67	0.19	0.19
	9-1	4.4	0.69	0.17	0.18
	10-2	4.2	0.66	0.16	0.16

Note: 1 ksi = 6.89 MPa.

ACKNOWLEDGMENTS

The author would like to thank S. Unjoh, Leader, Earthquake Engineering Team, Public Works Research Institute, Tokyo, Japan, for providing the Japanese publications.

REFERENCES

55. Kato, K., *Concrete Engineering Data Book,* Nihon University, Japan, 2000.

56. Kennedy, R. P., "A Statistical Analysis of Shear Strength of Reinforced Concrete Beams," PhD thesis, Department of Civil Engineering, Stanford University, Stanford, Calif., 1967.

57. Hedman and Losberg, A., "Design of Concrete Structures with Regards to Shear Forces," *Shear and Torsion*, Comité Euro-International du Béton (CEB), *Bulletin*, No. 126, Nov. 1978, pp. 184-209.

58. Kar, J. N., "Shear Strength of Prestressed Concrete Beams without Web Reinforcement," *Magazine of Concrete Research*, V. 21, No. 68, Sept. 1969, pp. 159-170.

59. Tanaka, Y., and Kishi, T., "Estimation Method of Shear Strength of RC Members Containing Artificial Crack or Unbonded Area," *Seisan Kenkyu*, V. 57, No. 2, 2005, pp. 107-110. (in Japanese)

AUTHORS' CLOSURE

The authors thank the discusser for his interest in this paper and for providing us with an opportunity to further clarify the concept of the proposed model. Each question and comment presented by the discusser is discussed separately as follows.

1. In the proposed method, the average compressive stress of the compression zone $\bar{\sigma}$ corresponding to beam shear failure shows a complicated trend. This is attributed to the fact that $\bar{\sigma}[\bar{\sigma} = \alpha_{x1}\varepsilon_o E_c/2]$ (Eq. (12)) is affected by various parameters (ρ, f_c', d, and h). Further, it should be noted that $\bar{\sigma}$ is affected by the shear demand as well as the shear capacity because it is determined at the intersection of the two curves (refer to Fig. 4). Therefore, the trend of $\bar{\sigma}$ cannot be directly evaluated by considering only a single design parameter.

For example, in the specimens of Ahmad and Lue[30] that the discusser mentioned, both the effective beam depth and tension reinforcement ratio of Beam C2 are different from those of Beams A2 and A8; Beam C2 has the least effective depth among the three specimens while having the highest tension reinforcement ratio. In such a case, the combined effect of the two parameters needs to be considered in the evaluation of $\bar{\sigma}$. The higher tension reinforcement ratio increases the (flexural) stiffness of the shear demand curve. Therefore, the shear failure of Beam C2 with the higher tension reinforcement ratio can occur with a less normal stress $\bar{\sigma}(= \alpha_{x1}\varepsilon_o E_c/2)$ (refer to Fig. 4 in the original paper). On the other hand, the shallow beam depth decreases the stiffness of the shear demand curve, which increases the normal stress $\bar{\sigma}$ corresponding to shear failure. In the authors' opinion, regarding the adverse effects of the two design parameters, the $\bar{\sigma}$ value of Beam C2 having the least effective beam depth and greatest tension reinforcement ratio between those of A2 and A8 is not unusual.

Also, it should be noted that the trend of $\bar{\sigma}$ is not always consistent with that of the shear strength of beam. Higher f_c' increases both the $\bar{\sigma}$ value and the shear strength of the beam by increasing the tensile strength of concrete. On the other hand, a higher tension reinforcement ratio tends to decrease the $\bar{\sigma}$ value as previously mentioned, whereas it increases the beam shear strength by increasing the depth of the compression zone.

2. According to the suggestion by the discusser, the authors compared the predictions by the proposed model with the Hedman-Losberg model.[57] As the discusser indicated, the Hedman-Losberg model[57] is based on the results of the test specimens with broader ranges of design parameters. Figure A shows the shear strengths predicted by the Hedman-Losberg[57] model and the proposed strength model. As shown in the figure, the proposed method showed better predictions than the Hedman-Losberg model[57] did.

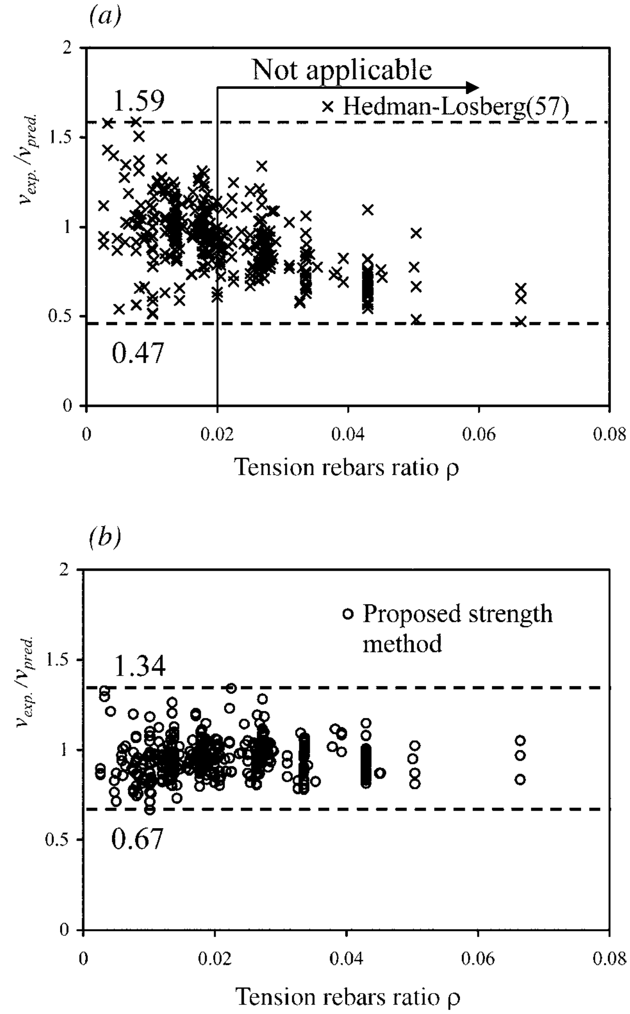

Fig. A—(a) Strength predictions by Hedman-Losberg model[57]; and (b) proposed strength model.

As the discusser indicates, the predictions by the Okamura and Higai model[11] (Fig. 10(c)) and Kim and Park model[23] (Fig. 10(g)) are as good as the predictions by the proposed model. The proposed strength model, however, not only shows good predictions, but also is based on a theoretical background. This is the advantage of the proposed model distinguished from other empirical models.

In this paper, the proposed model was verified for the test specimens with the ranges of $0.26 \le \rho \le 6.64$ (percent), $2.6 \le a/d \le 9.0$, $10.5 \le f_c' \le 104.2$ MPa ($1.5 \le f_c' \le 15.1$ ksi), and $69 \le d \le 1200$ mm ($2.7 \le d \le 47.2$ in.). The authors suggest that readers use the proposed model within the verification range.

3., 4., and 5. In the calculation of the depth of the compression zone at the critical section and loading point (c_{x1} and c_a), the nonlinearity of concrete stress was already considered. The parabolic distribution of compressive stress in the compression zone used in Eq. (6) represents approximately the nonlinearity and compression softening of concrete. Nevertheless, the authors agree that the equations proposed by the discusser may more accurately calculate the depth of compression zone and improve the predictability of the proposed strength model.

Disc. 103-S80/From the Nov.-Dec. 2006 *ACI Structural Journal*, p. 794

One-Way Shear Strength of Thick Slabs and Wide Beams. Paper by Edward G. Sherwood, Adam S. Lubell, Evan C. Bentz, and Michael P. Collins

Discussion by Himat Solanki

PE, Building Department, Sarasota County Government, Sarasota, Fla.

The authors have presented an interesting concept on one-way shear strength of thick slabs and wide beams with transverse reinforcement. The discusser would like to offer the following:

1. The authors have outlined nine test specimens in two test series in this paper. Out of nine test specimens, one specimen (AT-2/3000) has multiple loading conditions, whereas other specimens have a single concentrated load with a loading plate width either the full width of the beams or a partially-loaded width of the beams, that is, test Specimen AT-2/250A has a plate width of 152 x 152 mm (6 x 6 in.) that will not cover the full b_w, whereas test Specimen AT-2/250B will cover the full b_w. All nine specimens fall into three categories:

1. Specimens AT-2/250B, AT-2/1000A, and all specimens of test series three (AT3) could function as a one-way shear action;
2. Specimen AT-2/250A and AT-2/1000B could function as a partially two-way shear action; and
3. Specimen AT-2/3000 could function as a two-way shear action. In these specimens, the transverse (temperature and shrinkage) reinforcement was considered, but the amount of transverse reinforcement was not designed to ensure the sufficient load spreading action or action envisaged.

The authors have concluded from only two test specimens (AT-3C and AT-3D) that the transverse reinforcement in the slab does not alter the one-way shear stress at failure. Based on the authors' AT3 test series, test Specimens AT-3A and AT-3B show an influence (increase in shear stress capacity) due to transverse reinforcement. Test Specimens AT-3C and AT-3D have some unusual results even though the longitudinal reinforcement ratio and concrete compressive strength are identical. Therefore, the discusser believes that these two specimens are inconclusive. Regan and Rezai-Jorabi[18] and the Hillerborg[19] test series show that the transverse reinforcement would have a positive influence if it were properly designed for adequate load spreading action (test Specimens AT-2/250A, AT-2/1000B, and AT-2/3000).

The authors' Eq. (2) and supplementary Eq. (3) are based on the influence of crack spacing s_e and aggregate size a_g. Because the paper does not address the maximum aggregate size, it is very difficult to validate these equations. Also, these equations are contrary to some those of some researchers, such as Hillerborg[19] and Muttoni,[20] who have considered the crack width instead of crack spacing.

They have correlated the one-way shear strength of beam without shear reinforcement by considering the opening of a critical crack, and the failure of the beam was considered to be caused by the opening of a critical crack under increasing deformations.

Muttoni[20] has proposed the following equation based on the 269 test specimens

$$\frac{V_c}{b_w d\sqrt{f_c'}} = \frac{I}{3.0 + 7.7\varepsilon d k_{dg}}$$

where $\varepsilon d k_{dg}$ equals the nominal opening of a critical crack, in which ε is the longitudinal strain with respect to overall deflection and critical crack (based on Bernoulli's hypothesis for a cracked section); d equals the effective depth (mm); and $k_{dg} = 48/(D_{max} + 16)$ where D_{max} is the maximum aggregate size (mm).

Based on the previous equation, the approximate $\varepsilon d k_{dg} = 0.4$ value corresponds with the ACI code equation (Eq. (1)), and approximately 15% of the beams fall beyond the $\varepsilon d k_{dg} = 0.4$ value. If the mean value is considered from $0.0\varepsilon d k_{dg}$ to $0.4\varepsilon d k_{dg}$ values, the approximate shear stress would become $0.2\sqrt{f_c'}$, which is approximately 20% higher shear stress than the ACI code formula. The $0.2\sqrt{f_c'}$ value also corresponds if the authors' s_e value in Eq. (2) is considered a zero value (that is, $s_e = 0$).

The discusser has evaluated test results of Regan and Rezai-Jorabi,[18] Hillerborg,[19] and Aster and Koch[21] and has compared the results with the $0.2\sqrt{f_c'}$ value and found that the $0.2\sqrt{f_c'}$ value is consistent with the test results. In all previous test series, the concrete compressive strength f_c' varied from 27.6 to 44.9 MPa, which is also consistent with the authors' f_c' value.

It was noted that there are printing errors in Fig. 5 and 6. For example, the bottom last figures should be at the failure load of beams rather than intermediate applied load.

REFERENCES

18. Regan, P. E., and Rezai-Jorabi, H., "Shear Resistance of One-Way Slabs under Concentrated Loads," *ACI Structural Journal*, V. 85, No. 2, Mar.-Apr. 1988, pp. 150-157.

19. Hillerborg, A., "Förankringssäkerhet hos Konstruktioner utan Skjuvarmering," *Nordisk Betong*, No. 2, 1959, pp. 119-138.

20. Muttoni, A., "Schubfestigkeit und Durchstanzen von Platten ohne Querkraftbewehrung," *Beton und Stahbetonbau*, V. 98, No. 2, Feb. 2003, pp. 74-84.

21. Aster, H., and Koch, R., "Schubträgfahigkeit dicker Stahlbetonplatten," *Beton und Stahlbetonbau*, No. 11, Nov. 1974, pp. 266-270.

AUTHORS' CLOSURE

The discusser is thanked for his interest in this paper.

1. The experiments reported in this paper were designed to examine the one-way shear strength of reinforced concrete members. Rather than simply testing all specimens with full-width supports, it was decided to investigate the influence of different-width supports as well. This would simulate the effect of column supports rather than wall supports and increase the generality of any conclusions based on the test results. As noted in the paper, the ACI 318 code requires the determination of shear strengths against both beam action shear failures (one-way) and punching shear failures (two-way). The former failure mode was predicted by the ACI code to control all specimens, and the failure surface in Fig. 7 shows that this was correct for the widest specimen. Indeed, this was also true for all other specimens reported in the paper. Because all the AT-2 series specimens failed within ±5% of the average observed shear stress independently of the member or support width, it can be concluded that the

support width and member width had no significant effect on the shear strength in these tests. The ACI code implies that the clearly slab-like 10 ft (3.1 m) wide specimen should have a reliable shear strength approximately twice that of the beam-like 10 in. (254 mm) wide specimens. This was not observed and suggests that the code language distinction between a beam and a slab may be more of a terminological convenience than something based on physical behavior.

The discusser notes that the temperature and shrinkage steel was not designed for two-way action. This is correct and, as the strains in these bars were observed to be small, similar to those shown in Fig. 9, it can be concluded that the addition of more reinforcement in the transverse direction would not have resulted in different shear behavior. Shrinkage and temperature reinforcement were provided in five of the nine specimens reported in this paper and the shear behavior of these specimens did not consistently or significantly differ from those that did not contain this reinforcement.

2. The discusser is correct that this paper does not attempt to validate the influence of depth or aggregate size on shear strength and he is directed to References 4 and 22 for this discussion. The discusser states that a shear stress at shear failure of $0.2\sqrt{f_c'}$ is consistent with the test results that he has examined. With regard to this, it is worth noting that the average shear strengths of the AT-3, AT-2, and AT-1 series[4] of specimens failed at shear stresses of $0.19\sqrt{f_c'}$, $0.17\sqrt{f_c'}$, and $0.09\sqrt{f_c'}$, respectively. The effective depths of these series were 307, 439, and 925 mm (12, 17, and 36 in.), respectively, indicating that deeper members fail at lower shear stresses whether they are called beams or slabs.

3. Figures 5 and 6 are correct and show that the final crack pattern in a reinforced concrete member occurs after the peak load has already been attained and the member is in the post-peak domain.

REFERENCES

22. Sherwood, E. G.; Bentz, E. C.; and Collins, M. P., "The Effect of Aggregate Size on the Beam-Shear Strength of Thick Slabs," *ACI Structural Journal*, V. 104, No. 2, Mar.-Apr. 2007, pp. 180-190.

Disc. 103-S81/From the Nov.-Dec. 2006 *ACI Structural Journal*, p. 803

On the Stress in Unbonded Tendons at Ultimate: Critical Assessment and Proposed Changes. Paper by Mohamed H. Harajli

Discussion by Jinsheng Du and Pinyin Lu

Associate Professor, School of Civil Engineering, Beijing Jiao Tong University, Beijing, China; and Senior Engineer, First Highway Survey and Design Institute of China, Xi, China

The paper is interesting, as it again pointed out and verified that the equivalent plastic hinge length L_p is the most important parameter influencing stress f_{ps} in unbonded tendons at ultimate. Concerning the equivalent plastic hinge length and the stress increase in unbonded tendons at ultimate, the following points deserve discussion:

1. When the load type effect is included in the prediction equation for L_p or f_{ps}, it may cause confusion in the use of the equation because, in the ultimate limit state of a highway bridge, it is difficult for designers to judge (a) if one-point, 2/3-point, or uniform loading should be chosen; and (b) the loading arrangements in continuous beams. In addition, tests indicated that the stress increase in unbonded tendons at ultimate was not consistently higher for beams loaded with 2/3-point loading compared with beams with a single midspan point loading.[9] The discussers advocate the treatment of L_p according to Tam and Pannell's method, namely, L_p/c is taken as approximately 10. The method has been proven simple and reasonable[30];

2. The discussers believe the differences in techniques and methods of measurement, variation of material properties, and failure criteria of the specimens adopted by different investigators may cause the spread of the test results. These differences may also make most proposed equations, which are mainly based on data regression analysis, encounter significant scatter in the prediction of stress increase in unbonded tendons at ultimate. There is, however, a common phenomenon that exists in almost all test data performed by different investigators: the value of L_p/c tends to be constant in a specific series of tests. Therefore, L_p/c is a convenient parameter to judge how conservative the prediction equation is; and

3. Regarding Eq. (12), which was proposed by Lee et al.,[13] it should point out that in most cases, A_s' is less than A_s, the third term on the right-hand side of the equation would be minus. In some cases, the second term together with the other terms on the right-hand side of the equation may result in the stress f_{ps} in unbonded tendons at ultimate being smaller than their corresponding effective prestress f_{pe}. This is not correct in practice.

REFERENCES

30. Au, F. T. K., and Du, J. S., "Prediction of Ultimate Stress in Unbonded Prestressed Tendons," *Magazine of Concrete Research*, V. 56, No. 1, Feb. 2004, pp. 1-11.

AUTHOR'S CLOSURE

The author would like to thank the discussers for their interest in the paper and for their constructive comments.

As clearly stated in the paper, the purpose of the study was to conduct an objective assessment of the main parameters that influence the increase in stress Δf_{ps} in unbonded tendons at ultimate and to explain the reasons behind the scatter of the test data. In fact, because of this scatter, it would be hard to draw accurate conclusions about the effect of load application or any other parameter before a large body of test data is analyzed as undertaken in the subject study. Based on the results of this analysis, in accordance with the trend of test data shown in Fig. 5 to 7 and the derived Eq. (23) of the paper, there is a clear evidence to suggest that the type of load application influences the equivalent plastic hinge length and consequently influences Δf_{ps}. It should be noted that it is not only the equivalent plastic hinge length L_p that influences the stress results; but also the number n_p of the plastic hinges that develop in the process of forming a collapse mechanism and, most importantly, the ratio of the total equivalent plastic hinge length to the total length of the tendons between anchorages n_pL_p/L_a. Consequently, under a given type of load application (single concentrated or uniform), the value of n_pL_p/L_a when one span is loaded to form a collapse mechanism in multi-span (continuous) members is generally less when compared with simply supported members. The corresponding difference grows larger as the number of spans increases. Therefore, unnecessarily neglecting the member continuity would produce unconservative Δf_{ps} results.

On the other hand, the author agrees with the discussers that it would be easier for design purposes to consider one common and conservative type of load application. In this regard, it is worth mentioning that the author has already recommended that Joint ACI-ASCE Committee 423 adopt Eq. (27) of the paper for replacing Eq. (18-4) and (18-5) of the ACI Building Code (recommendation is currently under evaluation by Joint ACI-ASCE Committee 423). In adopting this equation, it is suggested that the number of plastic hinges n_p appearing in Eq. (28) of the paper be defined as $n_p = 1 + N_s/2$, where N_s is the number of support hinges required to form a collapse mechanism crossed by the tendon, which is similar to the definition adopted by the current AASHTO LRFD. In accounting for the effect of loading type, however, the author has further suggested that Joint ACI-ASCE Committee 423 consider the use of either $f = \infty$, which corresponds to the most conservative single concentrated load application, or $f = 6$, which corresponds to the more reasonable uniform load application.

Regarding Eq. (12) by Lee et al., the discusser agrees that the equation may lead to values less than the effective prestress f_{pe}, which is unrealistic. This inconsistency, however, may arise for all design expressions presented and compared in the paper, particularly when the area of the prestressing steel and/or the tension reinforcing steel are significantly high to produce a neutral axis depth c at ultimate exceeding the depth d_p of the tendons. This problem can easily be solved by imposing a minimum value on $f_{ps} = f_{pe}$.

Disc. 103-S82/From the Nov.-Dec. 2006 *ACI Structural Journal*, p. 813

Minimum Transverse Reinforcement for Bottle-Shaped Struts. Paper by Michael D. Brown and Oguzhan Bayrak

Discussion by Dipak Kumar Sahoo, Bhupinder Singh, and Pradeep Bhargava

Research Scholar, Assistant Professor, and Professor, Department of Civil Engineering, Indian Institute of Technology Roorkee, Roorkee, India.

The authors are to be complimented for their thorough and meticulous investigation of the necessity and the amount of transverse reinforcement in bottle-shaped struts.

The discussers would like to draw attention to two important issues related to the strut-and-tie modeling of bottle-shaped struts, namely, the location of the ties and the angle of dispersion of compression. The former issue is particularly relevant given the fact that in the ACI 318-05 specified dispersion model, the location of the ties in the strut-and-tie model for a bottle-shaped strut is not specified.

On the basis of isolated strut tests, Brown et al.[36] have reported that the first sign of distress in their square panels was in the form of a vertical crack that formed at the center at the midheight of the panels. As the load increased, the vertical crack propagated toward the top and bottom loaded edges of the panels. This implies that, during the initial stages of loading, the maximum transverse tensile strains occurred at the midheight of the panels. Therefore, the strut-and-tie model of Fig. 5(a) is a better representation of the force system within the bottle-shaped strut during the initial stages of loading. On the basis of the stress distribution proposed by Guyon,[1] the authors have suggested that the strut-and-tie model of Fig. 5(b) is the best representation of the force system within a bottle-shaped strut. It may be pointed out that for the full development of Guyon's stress trajectories, the length of the bottle-shaped strut has to be at least twice the maximum width available for the strut (Fig. 2). This, however, may not be obtained in practice all the time. Considering the fact that the location of the ties within the bottle-shaped strut is influenced by factors such as the length and width of the strut, the size of the bearing plates, and the stage of loading, the strut-and-tie model of Fig. 5(b) may not always be the best representation of the force system within a bottle-shaped strut.

It is suggested herein that the location of the tie in the strut-and-tie model for a bottle-shaped strut may not be that significant. This is because, irrespective of the location(s) of the tie(s) in any of the models of Fig. 5, the total tensile force in the ties works out to be 1/2 of the axial force in the strut, F_{strut}. At the same time, the nonstationary location of the tie at different stages of loading further diminishes the need for specifying tie location within a bottle-shaped strut.

The m:1 dispersion of compression within the bottle-shaped strut gives a transverse tensile force of F_{strut}/m in the tie. ACI 318-05 recommends 2:1 (m = 2) dispersion that will yield a transverse tensile force of $F_{strut}/2$ for which sufficient reinforcement has to be provided so as to maintain equilibrium in the strut. Given this relatively high reinforcement requirement based on equilibrium considerations, one wonders as to how ACI 318-05 can allow unreinforced bottle-shaped struts in the first place.

The authors may like to verify the consistency of their Eq. (1) and (2) derived from the model proposed by Schlaich and Weischede.[3] For example, when $l/3 = b_{min}$, $b_{ef} = l/3$ as per Eq. (1) and $l/2$ as per Eq. (2). This contradiction needs to be resolved.

For the square panels of Brown et al.,[36] in which $b_{min} = l/3$, the value of m estimated using Eq. (2) and (3) works out to be 6. It is thus obvious that for a length of the bearing plates equal to or less than 1/3 the axial length of the bottle-shaped strut, m has a minimum value of 6. In other words, for any length of the bearing plate up to 1/3 of the strut length, the magnitude of the transverse tensile force is equal to 1/6 of the axial force F_{strut}. On the basis of Eq. (2) and (3), it can be verified that, as the length of the bearing plate increases beyond 1/3 of the strut length, the transverse tensile force reduces. On the basis of the dispersion proposed by Guyon,[1] however, it is observed that the transverse tensile force reduces from a maximum magnitude of 3/10 of the axial force F_{strut} to zero as the length of the bearing plate b_{min} increases from zero to the full width of the isolated strut panel. The authors may like to comment on this disparity in the estimation of the transverse tensile force, and hence m, in a bottle-shaped strut.

The authors have made a graphical comparison in Fig. 10 of the provisions in A.3.3 and A.3.3.1 of ACI 318-05, Appendix A. In this figure, on the basis of Eq. (7), the reinforcement ratio $\rho_{\perp}$ is plotted against the slope of the angle of dispersion m. By rearranging the terms and considering the ACI 318-05 allowable maximum value for v = 0.85 × 0.75 = 0.64, Eq. (7) can be rewritten as

$$\rho_\perp \geq \frac{0.64}{m}\frac{f_c'}{f_y}\left(\frac{A_c}{bl}\right) \tag{10}$$

In the previous equation, by substituting appropriate values for f_c' and f_y, the required reinforcement $\rho_\perp$ can be expressed as a function of m and can be plotted for various (A_c/bl) ratios. The authors may wish to consider the option of using (A_c/bl) instead of (A_c/bl) in Fig. 10.

REFERENCES

36. Brown, M. D.; Sankovich, C. L.; Bayrak, O.; and Jirsa, J. O., "Behavior and Efficiency of Bottle-Shaped Struts," *ACI Structural Journal*, V. 103, No. 3, May-June 2006, pp. 348-355.

Disc. 103-S82/From the Nov.-Dec. 2006 *ACI Structural Journal*, p. 813

Minimum Transverse Reinforcement for Bottle-Shaped Struts. Paper by Michael D. Brown and Oguzhan Bayrak

Discussion by Mikael W. Braestrup

Senior Engineer, MSc, PhD, RAMBOLL, Copenhagen, Denmark

The discusser agrees with the authors' observation that reinforcement is necessary transverse to the axis of bottle-shaped struts to control cracks widths under service loads, but must take issue with the way in which they determine such reinforcement.

The reinforcement ratio $\rho_\perp$ perpendicular to a crack at the inclination is evaluated by Eq. (4) as $\rho_\perp = \rho_V\cos\theta + \rho_H\sin\theta$, with ρ_V and ρ_H being the reinforcement ratio in the vertical and the horizontal direction, respectively. As correctly stated in the preceding text, in accordance with the coordinate transformation described by Mohr's circle, the trigonometric functions should be squared. In the discusser's opinion, this has nothing to do with shear slip along the crack but is a simple consequence of equilibrium. Indeed, for Eq. (4), with the first power trigonometric functions to be valid, the reinforcement should be kinked perpendicular to the crack, which is totally unrealistic. As a consequence of Eq. (4), the contribution of skew reinforcement is seriously overestimated (by 41% for θ = 45 degrees).

This is precisely the case for the described beam tests. The assumed value of θ is not stated; but judging from the numbers, it would be 45 degrees, with $\rho_V = \rho_s$ = 0.0022 for Specimen I-UL-17-0 and $\rho_V = \rho_s$ = 0.0043 for Specimen I-UL-8.5-0b. (The authors should state the cross-sectional area of used reinforcement, or at least provide an identification more revealing than "No. 3 bar.") The discusser has calculated the corresponding reinforcement ratios across the crack to be $\rho_\perp$ = 0.0011 and $\rho_\perp$ = 0.0022, and not $\rho_\perp$ = 0.0015 and $\rho_\perp$ = 0.003, respectively.

The required reinforcement ratio is then evaluated by Eq. (8) as $\rho_\perp = P_u/(f_y bl\cot\phi)$ where b is the width of the beam, l is the total length of the strut, and ϕ is the angle of dispersion of the strut compression. The force P_u is not defined, but presumably it is the design axial load on the strut. Equation (8) would seem to be at variance with the preceding discussion, where St. Venant's principle is invoked to demonstrate that transverse reinforcement is only needed for a distance of one member depth from the application of the strut force, and not over the entire length of the strut. That would not matter if Eq. (8) was used to determine the required reinforcement ratio, which then was placed over the dispersion length only, but that does not seem to be the case.

The aforementioned considerations cast some doubt on the validity of the conclusions of the paper, but apparently the over-estimation of the reinforcement strength would exacerbate the claimed inconsistency of the ACI 318-05 recommendations.

Disc. 103-S82/From the Nov.-Dec. 2006 *ACI Structural Journal*, p. 813

Minimum Transverse Reinforcement for Bottle-Shaped Struts. Paper by Michael D. Brown and Oguzhan Bayrak

Discussion by Sung-Chul Chun, Taehun Ha, Sung-Gul Hong, and Bohwan Oh

Principal Researcher, Daewoo Institute of Construction Technology, Suwon, Korea; Senior Researcher, Daewoo Institute of Construction Technology; Associate Professor, Department of Architecture, Seoul National University, Seoul, Korea; and Chief Researcher, Daewoo Institute of Construction Technology

The authors have presented an interesting and valuable concept on the minimum transverse reinforcement for bottle-shaped struts. The discussers would like to offer the following comments:

1. As the authors pointed out, the equivalent resisting force perpendicular to the crack $F_\perp$ in Fig. 8 is related to the equivalent reinforcement ratio perpendicular to the expected splitting crack $\rho_\perp$ by Eq. (5). Substituting Eq. (4) into Eq. (5), however, does not yield the equation for $F_\perp$ in Fig. 8. The reason for this inconsistency is that the resisting force $F_\perp$ in Fig. 8 was defined as a sum of forces from one vertical and one horizontal shear reinforcement. The resisting force $F_\perp$ should be defined as total resisting force along the entire length of expected crack to resist the total tensile force T as shown in Fig. 7. The correct resisting force $F_{\perp,correct}$ can be expressed as Eq. (11) including the numbers of reinforcing bars in two orthogonal directions along expected splitting crack.

$$\begin{aligned} F_{\perp,correct} &= n_V A_V f_y \cos\theta + n_H A_H f_y \sin\theta \\ &= \frac{A_V f_y l\cos^2\theta}{s_V} + \frac{A_H f_y l\sin^2\theta}{s_H} \end{aligned} \tag{11}$$

where $n_V = (l\cos\theta)/s_V$ and $n_H = (l\cos\theta)/s_H$ are the numbers of vertical and horizontal reinforcing bars along expected splitting crack, respectively. Now the correct equivalent ratio can be obtained from Eq. (5) and (11).

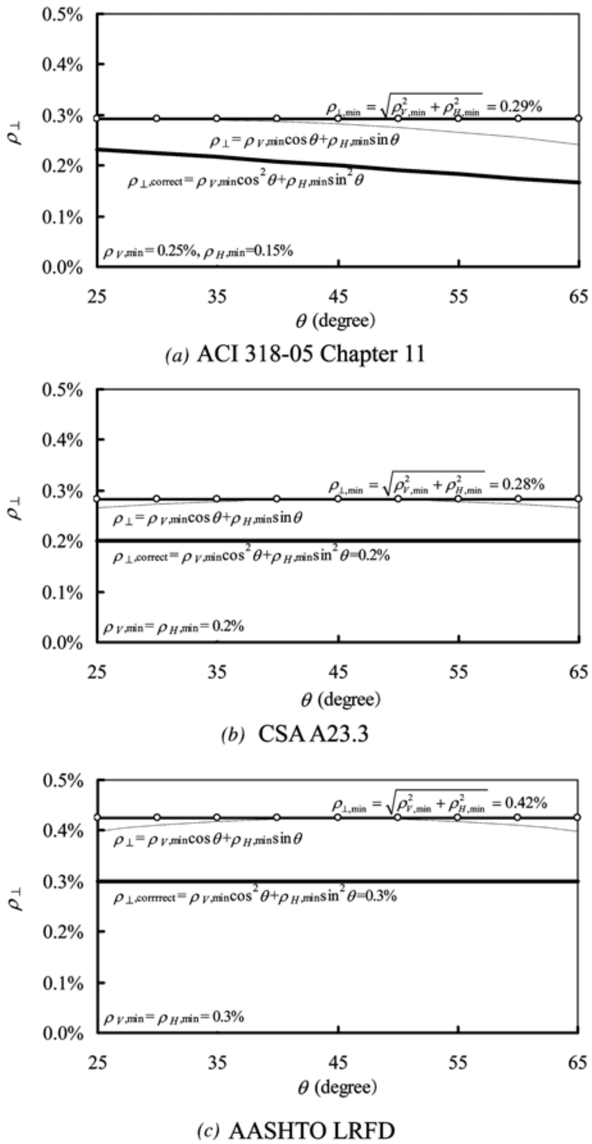

Fig. A—Comparisons of $\rho_{\perp,\min}$, $\rho_\perp$, *and* $\rho_{\perp,\mathrm{correct}}$.

$$\rho_{\perp,\,correct} = \frac{F_{\perp,\,correct}}{f_y bl} = \frac{A_V\cos^2\theta}{bs_V} + \frac{A_H\sin^2\theta}{bs_H} \qquad (12)$$

A similar equation may also be found from Reference 37, which was derived using the usual transformation formulas for plane stress fields.

2. Based on a similar speculation, it is found that the formula in the commentary for Section A.3.3.1 in ACI 318-05 has an error in the power of the trigonometric function $\sin\alpha_i$. It should be expressed as

$$\frac{A_{si}f_{si}}{b_s s_i}\sin^2\alpha_i \qquad (13)$$

Consequently, Eq. (A-4) of ACI 318-05 (Eq. (9) in the paper) may be amended as

$$\sum\frac{A_{si}}{b_s s_i}\sin^2\alpha_i \geq 0.003 \qquad (14)$$

The value of 0.003 was not clearly explained in the paper and the code commentary.

3. The SRSS (square root of the sum of the squares) method was used to compare the minimum reinforcement ratios of the four provisions, that is, Section A.3.3.1 and Chapter 11 of ACI 318-05, CSA A23.3, and AASHTO LRFD. The discussers calculated the equivalent reinforcement ratios using the SRSS method, Eq. (4), and Eq. (12) with varying angles between expected splitting cracks and longitudinal reinforcement. Figure A shows that the SRSS method provides upper bound values. Especially, compared with the values calculated by the correct equivalent reinforcement ratio (Eq. (12)), the SRSS greatly overestimates the minimum reinforcement ratios. It is not reasonable to use the SRSS method to calculate the equivalent reinforcement ratios in the perpendicular direction to possible splitting cracks in orthogonally reinforced concrete members.

REFERENCES

37. Nielsen, M. P., *Limit Analysis and Concrete Plasticity*, CRC Press, Boca Raton, Fla., 1999, pp. 93-98.

AUTHOR'S CLOSURE

The authors thank the discussers for their interest in the paper and critical evaluation of the work presented therein. The authors agree with the discussers that the use of bottle-shaped struts without transverse reinforcement as allowed by Appendix A of ACI 318-05 is not recommended, as stated in the first conclusion of the paper. Additional closures to each of the three discussions are presented as follows.

Closure to discussion by Sahoo, Singh, and Bhargava

Strut-and-tie modeling is based on, and requires, plastic redistribution in the members being modeled. When a member is undergoing plastic redistributions, load is distributed according to strength as opposed to elastic deformations where load is distributed according to stiffness. As the concrete panels presented in Reference 36 cracked, the reinforcing bars in them became the stronger elements and began to attract load. Thus, if reinforcement is placed within the panels, plastic redistribution will cause a cracking pattern and force distribution to take advantage of those bars. The presence or absence of bars at midheight will not significantly affect the formation of the vertical cracks that occurred in the panels reported in Reference 36. Hence, the authors agree with the idea that the transverse ties in a bottle-shaped strut should not be fixed at a single location. Doing so would limit the adaptability of strut-and-tie modeling. Adaptability is one of the primary advantages of the method. The centroid of the reinforcement placed in a member, however, should coincide with the assumed tie location.

The discussers are correct that there is a discontinuity present in Eq. (1) and (2). Discontinuities of this nature, however, occur whenever a complex continuous phenomenon is modeled with a simple step function. The authors did not conduct an in-depth examination of the dispersion of the compression in a bottle-shaped strut, but rather adopted a sufficiently simple, existing model.[3] Equation (8) is presented with the value m as an input parameter so that practitioners can apply any value of slope they deem appropriate. That value of slope need not be determined using either the model presented by Schlaich and Weischede,[3] Guyon,[1] or the value of 2 suggested by ACI 318-05.[2] In fact, Schlaich et al.[38] recommend that the value of m be determined from an elastic finite element analysis.

The requested alterations to Fig. 10 have been made and are incorporated into Fig. B. The authors see no significant difference between Fig. 10 and B.

Closure to discussion by Braestrup

It is the authors' understanding that the development of the minimum reinforcement for a bottle-shaped strut as presented in Section A.3.3.1 of ACI 318-05 begins by assuming that there is a single reinforcing bar that is perpendicular to the splitting crack in a strut. If that crack opens without any shear slip, that reinforcing bar will be in a state of pure tension. Inclined shear reinforcement, however, is rarely used in North American practice. To address the common use of an orthogonal grid, Eq. (A-4) of ACI 318-05 (Eq. (9) of the paper) was developed. This equation takes the components of the bars comprising the orthogonal grid that are perpendicular to the crack. When using an orthogonal grid of bars, however, the bars must kink as the crack opens regardless of the no shear-slip assumption. The discusser is correct that if the squares of the sine terms are used, the values reported for Specimens I-UL-8.5-0b and I-UL-17-0 change from 0.0015 and 0.003 (as reported in the paper) to 0.0011 and 0.0022 (as presented by the discusser). The discusser is right that to be technically correct, the trigonometric terms shown in Eq. (9) should be squared, as stated in our paper and quoted by the discusser:

> When these forces are considered and their interaction is examined using Mohr's Circle for stress, the trigonometric functions shown in Fig. 8 should be raised to the second power rather than to the first power as shown.

The authors have chosen, however, not to square those terms to be consistent with the procedures and equations presented in ACI 318-05.

The database of specimens presented in this paper was assembled only from tests of beams with shear span-to-depth ratios of 2 or less. All inclined struts are located entirely within D-regions because the St. Venant's principle would apply to the local disturbance at the reaction and at the applied load. If those two disturbances are separated by a distance less than or equal to twice the member depth, the entire strut is located in a zone that is subject to St. Venant's principle. If one chooses to apply strut-and-tie modeling to a beam member with a shear span-to-depth ratio greater than 2, there would be a B-region between the D-regions associated with the applied load and reaction. The reinforcement requirements presented in the paper are intended to apply only to D-regions. The reinforcement specified in Chapter 11 of ACI 318-05 should be used for a B-region.

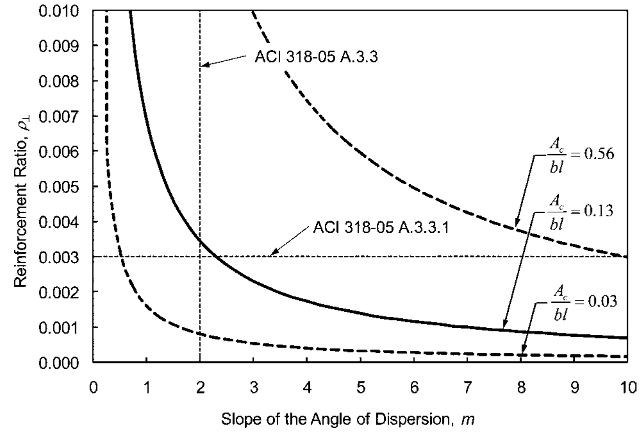

Fig. B—Variations in required reinforcement for various A_c/bl *values.*

Closure to discussion by Chun, Ha, Hong, and Oh

Quoting from the our paper: "When [the forces on the bars] are considered and their interaction is examined using Mohr's Circle for stress, the trigonometric functions shown in Fig. 8 should be raised to the second power rather than to the first power as shown." To be consistent with the current ACI 318 design provisions, the authors chose not to square the trigonometric functions.

FINAL WORDS

As described in the original paper and recognized by the discussers, minimum transverse reinforcement requirements of Appendix A of ACI 318-05 provisions can be improved. The first conclusion of the paper highlights the most serious shortcoming of the Appendix A provisions: unreinforced bottle-shaped struts. As can be inferred from Fig. 9 and 11, the actual amount of reinforcement required to keep a bottle-shaped strut in equilibrium is sufficiently small for most of the test specimens examined in the paper, regardless of the fact that the trigonometric functions are squared or not. In conclusion, we would like to reiterate parts of the two conclusions of our paper:

- "…The use of a variable angle of dispersion often requires a reinforcement ratio less than 0.003. However, considerations for serviceability must also be made…" and
- "…Additional research regarding the serviceability of structures designed using strut-and-tie provisions is needed…"

REFERENCES

38. Schlaich, J.; Schäfer, K.; and Jennewein, M., 1987, "Towards a Consistent Design of Structural Concrete," *PCI Journal*, V. 32, No. 3, pp. 74-150.

Disc. 103-S83/From the Nov.-Dec. 2006 *ACI Structural Journal*, p. 822

Behavior and Design of Adhesive Bonded Anchors. Paper by Rolf Eligenhausen, Ronald A. Cook, and Jörg Appl

Discussion by Shiming Chen

Professor, School of Civil Engineering, Tongji University, Shanghai, China

The discusser appreciates the authors' comprehensive work to simulate the behavior of adhesive bonded anchors based on a broad range of test data. Some findings are interesting to the discusser; however, they were not well clarified. Discussions are as follows.

Influence of bond strength of adhesive

It is not well evaluated how the bond strength of the adhesive influences the failure mode. As the mean bond strength at the adhesive/anchor interface for individual products ranges from 330 to 2830 psi (2.3 to 19.5 MPa), this

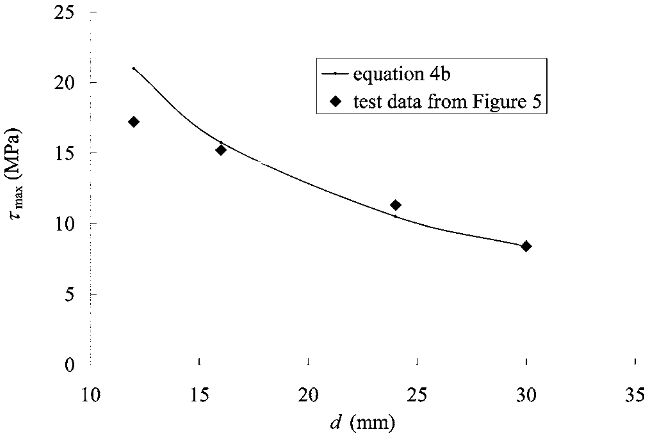

Fig. A—Comparison of shear bond stress against diameter of anchor.

should have great influence on the breakout failure of the anchors as expressed in Eq. (1b) for post-installed mechanical anchors. Equations (4a) and (4b) are derived from equilibrium of a bonded anchor using a uniform bond stress model. As far as the bond strength of the adhesive is greater than the maximum bonded stress (expressed as Eq. (4a) or (4b)), the concrete breakout capacity is determined for a single anchor.

Figure 5 illustrates that when the diameter is larger than 16 mm (0.6 in.), the failure load is governed by the breakout failure of concrete and agrees well with the predicted values (Eq. (1b)). A comparison of the shear bond stress derived from Eq. (4b) and from the test values (given in Fig. 5) is given in Fig. A. Accordingly, the failure loads of the tested anchors are all limited to the breakout failure of concrete, but the mean bonded shear stress varies with the diameter of the anchors. As the same mortar and the same embedment depth were adopted, it is likely that the shear bond strength at the adhesive/anchor interface required to secure a concrete breakout failure drops as the diameter of the anchors increases. It fails to reach the expected the failure load expressed by Eq. (1b) (a decrease by 20%), however, when the diameter of the anchors is 12 mm (0.47 in.), and the shear bond stress is 2500 psi (17.2 MPa), as illustrated in Fig. 5. In designs using post-installed adhesive anchors, it is understood that the embedment depth of an adhesive anchor, in terms of a multiple of the anchor diameter, is a key factor in governing of the breakout failure of the anchors. The greater the embedment depth is, the failure load will be, as far as concrete breakout failure occurs; and it would be beyond practical understanding that the failure load of the anchors of 12 mm (0.47 in.) in diameter, with a ratio of embedment depth to diameter of 8.33, would be smaller than that of 24 mm (0.9 in.), with a ratio of embedment depth to diameter of 4.17. Can the authors clarify whether it is owing to the mean bond strength decrease as the anchor diameter increases, or the shear bond stress distributed more sharply at the adhesive/anchor interface, leading to a lower failure load?

A variation curve of shear bond stress against the diameter of the anchor based on Eq. (4) together with the test values derived from Fig. 5 is drawn in Fig. A. From Fig. A, it is expected if the bond strength at the adhesive/anchor interface is lower than the maximum stress, the pullout or the bond failure would occur, and this may govern the failure of the anchors.

Numerical model

A numerical study was carried out based on the three-dimensional nonlinear finite element analysis. It is indicated that the microplane model integrated the threads, and mortar behavior was adopted in the study. As the cited reference is written in German, can the authors further highlight its main features of the model so the reader can follow the mechanism and the failure criterion at the adhesive/anchor interface in the numerical study?

The failure loads based on the numerical study should correspond to different failure patterns, as graphically demonstrated in Fig. 6 and 7. It is not clear what role the variations in the spacing, the embedment, and the adhesive of anchors play in the governing failure patterns.

Figure 18 demonstrates a comparison of failure loads of anchor groups based on the test results, the numerical study, and Eq. (2a). It appears that the failure load of the anchor group increases with the increased spacing but is much lower than the concrete breakout failure load given by Eq. (2), even if the spacing is greater than the critical spacing s determined by either Eq. (5) or (9). Does it imply that it is unsafe to predict the failure load of adhesive anchors by Eq. (1) and (2), which are only valid for the post-installed mechanical anchors? If this is true, how is it explained in Fig. 5, when single adhesive anchors are used, that the failure loads agree well with the predicted values when the diameter of the anchors is greater than 16 mm (0.6 in.)?

Note: see also "Errata" on p. 647 of this issue.

ERRATA

Please make the following correction to the paper that appeared in the *ACI Structural Journal*, V. 103, No. 6, November-December 2006.

103-S83, "Behavior and Design of Adhesive Bonded Anchors" by Rolf Eligehausen, Ronald A. Cook, and Jörg Appl

p. 823.

Table 1(a) and (b): Change all instances of "max." to "min." and "min." to "max."